

# Critical Speed for the Dynamics of Truck Events on Bridges with a Smooth Road Surface

Arturo González <sup>1</sup>, Eugene J. OBrien <sup>2</sup>, Daniel Cantero <sup>3</sup>, Yingyan Li <sup>4</sup>, Jason Dowling <sup>5</sup>, Ales Žnidarič <sup>6</sup>

**Abstract:** Simple numerical models of point loads are used to represent single and multiple vehicle events on two-lane bridges with a good road profile. While such models are insufficiently complex to calculate dynamic amplification accurately, they are presented here to provide an understanding of the influence of speed and distance between vehicles on the bridge dynamic response. Critical combinations of speed as a function of main bridge natural frequency and meeting point of two vehicles travelling in opposite directions are identified. It is proposed that such simple models can be used to estimate the pattern of critical speeds versus dynamic amplification for heavy trucks on a bridge with a relatively smooth surface. The crossing of a three-dimensional spring-dashpot truck is simulated over a bridge plate model to test this hypothesis for a range of road roughness. Further validation is carried out using the site-specific mean pattern associated to field measurements due to the passage of a truck population. The latter is found to be closely resembled by the theoretical pattern derived from simple point load models.

**Keywords:** highway bridges; bridge loads; structural dynamics; traffic speed; dynamic amplification.

<sup>1</sup> College lecturer, UCD School of Architecture, Landscape and Civil Engineering, University College Dublin, Newstead, Dublin 4, Ireland. E-mail: [arturo.gonzalez@ucd.ie](mailto:arturo.gonzalez@ucd.ie), phone: +353-1-7163219, fax: +353-1-7163297

<sup>2</sup> Professor of Civil Engineering, UCD School of Architecture, Landscape and Civil Engineering, University College Dublin, Newstead, Dublin 4, Ireland. E-mail: [eugene.obrien@ucd.ie](mailto:eugene.obrien@ucd.ie), phone: +353-1-7163224, fax: +353-1-7163297

<sup>3</sup> Research Assistant, UCD School of Architecture, Landscape and Civil Engineering, University College Dublin, Newstead, Dublin 4, Ireland. E-mail: [daniel.cantero@ucd.ie](mailto:daniel.cantero@ucd.ie), phone: +353-1-7163233, fax: +353-1-7163297

<sup>4</sup> Research assistant, Arup Consulting Engineers, formerly University College Dublin, Dublin, Ireland. E-mail: [yingyan.li@gmail.com](mailto:yingyan.li@gmail.com)

<sup>5</sup> Research Assistant, UCD School of Architecture, Landscape and Civil Engineering, University College Dublin, Newstead, Dublin 4, Ireland. E-mail: [jason.dowling@ucd.ie](mailto:jason.dowling@ucd.ie), phone: +353-1-7163233, fax: +353-1-7163297

<sup>6</sup> Researcher, Slovenian National Building and Civil Engineering Institute, Dimiceva 12, SI-1000, Ljubljana, Slovenia. E-mail: [ales.znidaric@zag.si](mailto:ales.znidaric@zag.si), phone: +386-1-2804207, fax: +386-1-2804484

## Nomenclature

$a$	= roughness coefficient
$c$	= speed of the vehicle
$\mathbf{C}$	= damping matrix of bridge model
$d$	= distance between reference masses for two vehicles travelling in opposite direction
DAF	= dynamic amplification factor
$E$	= Young's modulus of beam
$f_1$	= first natural frequency of the bridge
FR	= frequency ratio
$g$	= acceleration due to gravity
$I$	= second moment of area of cross-section
IRI	= international roughness index
$j$	= mode number
$k$	= vehicle number
$\mathbf{K}$	= stiffness matrix of bridge model
$L$	= beam length
$\mathbf{M}$	= mass matrix of bridge model
$M(\xi, \tau)$	= dimensionless total bending moment
$M_{R_{ik}}(\xi, \tau)$	= dimensionless bending moment due to interaction forces $R_{ik}$
$M_{\mu}(\xi, \tau)$	= dimensionless bending moment due to bridge inertial forces
$\mathbf{p}$	= forcing vector

$P_{ik}$	= constant point load representing axle (or wheel) force $i$ in vehicle $k$
PSD	= power spectral density
$q_j(\tau)$	= normalised deflection for mode $j$ and instant $\tau$
$R_{ik}$	= dimensionless force corresponding to axle (or wheel) force $i$ in vehicle $k$
$t$	= time ( $t = 0$ when the vehicle is located at the start of the bridge)
$x$	= location of section under investigation from the start of the bridge
$x_{ik}$	= position of axle (or wheel) force $i$ in vehicle $k$ on the bridge ( $x_{ik} = 0$ when the force is located at the start of the bridge)
$v(x,t)$	= deflection of the beam at position $x$ and instant $t$
$\mathbf{v}$	= vector of nodal displacements and rotations
$\dot{\mathbf{v}}$	= vector of nodal velocities
$\ddot{\mathbf{v}}$	= vector of nodal accelerations
$W$	= bridge width
$\alpha$	= speed parameter $\left( \alpha = \frac{c}{2f_1L} \right)$
$\delta(x)$	= Dirac function (impulse, also known as delta function)
$\varepsilon_{ik}$	= parameter indicating whether the axle (or wheel) $i$ in vehicle $k$ is on ( $\varepsilon_{ik} = 1$ ) or off ( $\varepsilon_{ik} = 0$ ) the bridge
$\xi$	= normalised section location on the bridge. $\xi = \frac{x}{L}$ ( $0 \leq \xi \leq 1$ )
$\xi_{ik}$	= normalised position of $P_{ik}$ along the bridge. $\xi_{ik} = \frac{x_{ik}}{L}$ ( $0 \leq \xi_{ik} \leq 1$ )
$\tau$	= normalised time $\left( \tau = \frac{\pi c t}{L} \right)$
$\mu$	= mass per unit length of the bridge
$\zeta$	= damping ratio

$\omega_b$  = damped circular frequency of the beam  $\left(\omega_b = 2\pi f_1 \sqrt{1 - \zeta^2}\right)$

$\Omega$  = spatial natural frequency

$\vartheta$  = damping parameter  $\left(\vartheta = \frac{\omega_b}{f_1}\right)$

## 1. Introduction

For long-span bridges, the governing traffic loading condition consists of a queue of heavy vehicles on the bridge in congested or jammed conditions [1]. In such a case, it is assumed that there is no dynamic amplification of the static load. However, for short- to medium-span bridges, the governing condition is made of a small number of vehicles travelling at high speed and inducing vibration in the bridge. There is some debate as to whether bridge loading events involving three and four high-speed trucks can be expected to feature amongst the most critical loading conditions for two-lane medium-span bridges [2]. Even so, it is clear that single truck crossings and two-truck meeting events play an important role in the assessment of the traffic load for short and medium-span bridges.

While considerable research has been carried out on single truck crossing events on bridges [3-10], the dynamics of two-truck meeting events has received less attention [11-16]. Finite Element (FE) Vehicle Bridge-Interaction (VBI) models of meeting events can be constructed but are computationally expensive and they include a degree of uncertainty on many of the vehicle dynamic parameters, and in particular, those intervening in the critical meeting events. However, vehicle dynamic parameters

such as tire stiffness, suspension stiffness, damping or mass moment of inertia are less influential on the bridge response in the case of very good profiles and relatively long bridges. So, Brady and OBrien [12] have considered the case of two moving point (2P-) loads on a 1D simply supported beam. This is clearly simplistic as it fails to allow for the interaction between the truck and the bridge masses, the road surface profile and the truck suspension systems, to name just some parameters. Nevertheless, this simplified model can be used to find an explanation for the dynamic peaks generated at certain speeds.

The ratio of maximum total strain to maximum static strain is defined as Dynamic Amplification Factor (DAF). The goal of this paper is to use these simple P-load models to identify the vehicle speeds that will cause maximum DAFs in bridges with a smooth surface. A smooth surface is associated here to ‘very good’ and ‘good’ ISO road classes [17]. The investigation focuses on critical loading events consisting of the simultaneous crossing of two 5-axle semi-trailers over a two-lane simply supported bridge. This truck class is the most common heavy goods truck configuration on European and many international roads. The P-loads simulate vehicle forces of magnitude and spacing equivalent to those of the 5-axle vehicle, and they are crossed over two types of bridge models: a 1D beam and a 2D FE isotropic plate. First, two groups of five point (5P-) loads travelling on a beam in opposite directions are used to represent the axle forces of two 5-axle trucks meeting on a bridge. This is the first analysis which considers a full range of possible vehicle speeds and truck meeting points while taking into account of the axle weight distribution in a large truck. These critical speeds are also derived for the case of two groups of 10P-loads representing wheel forces of a 5-axle truck running on a FE plate model. The critical speeds

estimated based on simulations of P-loads are compared to the results of more sophisticated 3D spring-dashpot vehicle dynamic models over a range of ‘good’ road profiles and three medium span lengths. Finally, the approach is tested with strain measurements from a bridge located in Vransko, Slovenia. This field data has been collected during the European FP6 project ARCHES (Assessment and Rehabilitation of Central European Highway Structures, 2006-2009) [18]. Maximum total strain was measured on the site for single events of a truck fleet using the Bridge Weigh-In-Motion system known as Si-WIM [19]. For each traffic event, the static strain was extracted from the record of measured strain through a low-pass filtering technique. Finally, the experimental ‘DAF – speed’ pattern associated to a given vehicle subclass is compared to the theoretical pattern derived from equivalent P-load models.

## **2. Simulations using moving constant loads**

The influence of speed on DAF due to a typical European 5-axle truck is analysed for three medium-span bridge lengths. For this purpose, the passage of a series of P-loads is simulated over two types of bridge models: a 1D beam and a 2D isotropic plate. In the bridge plate model, each P-load represents a wheel force of magnitude equal to half the static axle weight and the effect of transverse position on the critical speed is addressed. The plate width  $W$  is assumed to be 15 m, the spacing between wheels of the same axle is 2 m, and the path of the inner wheels is offset by 1 m from the bridge centreline. To get representative dimensions and relative weights between axles for a typical 5-axle European truck, weigh-in-motion data from the national road RN23 at Angers, France, is employed [2]. The recorded mean axle spacings were 3.0 m between 1<sup>st</sup> and 2<sup>nd</sup> axle, 5.1 m between 2<sup>nd</sup> and 3<sup>rd</sup> axle and 1.1 m between

consecutive axles of the rear tridem. The mean axle weights were 12.70 percent, 27.70 percent, 19.86 percent, 19.87 percent and 19.87 percent of the gross weight for axles 1 to 5 respectively. The total mass of a single truck is assumed to be 48440 kg. Bridge responses and ‘DAF-speed’ patterns are also obtained for an articulated 5-axle sprung model running over a range of road profiles and allowing for VBI. These simulations are used to assess the influence of road roughness and VBI on the critical speed and how they compare to that ‘DAF-speed’ pattern suggested by simple P-load models. All vehicle and bridge simulation models have been built using Matlab [20].

## 2.1 Dynamic model based on P-loads running in opposite directions

Dynamic amplification is calculated for a series of moving point loads,  $P_{ik}$ , representing the static component of force  $i$  exerted by vehicle  $k$ , travelling at a speed  $c$  towards one another over a simply supported bridge model of length  $L$ . The simulations are carried out using 1D beam bridge models where  $P_{ik}$  will represent a vehicle axle force (Fig. 1(a)), and 2D plate bridge models where  $P_{ik}$  will represent a vehicle wheel force (Fig. 1(b)). For comparison purposes, those beam and plate bridge models with the same length  $L$ , have similar mechanical properties and longitudinal frequencies of vibration. It is assumed that both vehicles have the same speed, axle weights and spacings. The ratio  $d/L$  is employed to define the relative position of the loads when they meet on the bridge, where  $d$  is given by the distance of the 3<sup>rd</sup> axle of the second truck from the 3<sup>rd</sup> axle of the first truck when the latter is located at midspan (this is,  $d$  is defined as shown in Fig. 1(a) when  $x_{31} = L/2$ ). So,  $d/L = 0$  represents a situation where the first axle of each tridem meet at the center,  $d/L = 0.5$  is a situation where the tridem of the second truck is just arriving on the bridge while the tridem of the first vehicle is at midspan (so both tridems will meet at one quarter



of the span),  $d/L = 1$  is a situation where one tridem leaves the bridge at the time the other tridem is entering it, and for  $d/L > 1$  the tridems will not meet on the bridge.

[FIG. 1 HERE]

The solution for the case of a constant P-load moving over a 1D simply supported beam has been described in dimensionless modal form by Frýba [21], and for two vehicle models consisting of 5P-loads each (Fig. 1(a)), it is given by:

$$\frac{\partial^2 q_j(\tau)}{\partial \tau^2} = \frac{\pi^2}{\alpha^2} \sum_{k=1}^2 \left( \sum_{i=1}^5 \varepsilon_{ik} R_{ik} \sin(j\pi \xi_{ik}) \right) - j^4 \frac{\pi^2}{\alpha^2} q_j(\tau) - \frac{\vartheta}{\alpha} \frac{\partial q_j(\tau)}{\partial \tau} \quad j = 1, 2, \dots \quad (1)$$

where  $q_j(\tau)$  is the  $j^{\text{th}}$  modal coordinate of the beam deflection;  $j$  is the mode number;

$\tau$  is the dimensionless time ( $\tau = \frac{\pi c t}{L}$  where  $t$  is time and  $L$  is bridge length);  $\alpha (= \frac{c}{2f_1 L})$

where  $f_1$  is the first natural frequency of the bridge) and  $\vartheta (= \frac{\omega_b}{f_1})$  where  $\omega_b$  is damped

circular frequency of the bridge) represent speed and damping parameters

respectively;  $\varepsilon_{ik}$  can be 1 or 0 depending if a particular load  $P_{ik}$  is on or of the beam

respectively;  $\xi_{ik}$  is the dimensionless position of  $P_{ik}$  ( $\xi_{ik} = \frac{x_{ik}}{L}$  where  $x_{ik}$  is the position

of  $P_{ik}$  with respect to the point of entrance of the vehicle  $k$  on the bridge); and the

dimensionless force  $R_{ik}$  is given by:

$$R_{ik} = \frac{P_{ik}}{\sum_{k=1}^2 \left( \sum_{i=1}^5 P_{ik} \right)} \quad i = 1, 2, \dots, 5; \quad k = 1, 2 \quad (2)$$

Eq. (1) is solved numerically using the Runge-Kutta-Nyström method with  $R_{ik}$  estimated as in Eq. (2). Values for  $\ddot{q}_j(\tau)$ ,  $\dot{q}_j(\tau)$ , and  $q_j(\tau)$  are obtained for each mode of vibration  $j$  at each instant in time,  $\tau$ . The total dimensionless bending moment,  $M(\xi, \tau)$  at normalized beam location  $\xi$  and normalized time  $\tau$  can be obtained from the sum of two dimensionless bending moments:  $\sum_{k=1}^2 \left( \sum_{i=1}^5 M_{R_{ik}}(\xi, \tau) \right)$  due to the applied loads and  $M_\mu(\xi, \tau)$  due to the vibration of the bridge as defined in Eqs. (3), (4) and (5).

$$M(\xi, \tau) = \sum_{k=1}^2 \left( \sum_{i=1}^5 M_{R_{ik}}(\xi, \tau) \right) + M_\mu(\xi, \tau) \quad (3)$$

where:

$$M_{R_{ik}}(\xi, \tau) = \begin{cases} = 4\varepsilon_{ik} R_{ik} (1 - \xi_{ik}) \xi & \text{for } \xi_{ik} \geq \xi \\ = 4\varepsilon_{ik} R_{ik} (1 - \xi) \xi_{ik} & \text{for } \xi \leq \xi_{ik} \end{cases} \quad (4)$$

and

$$M_\mu(\xi, \tau) = -\frac{1}{12} \alpha^2 \sum_{j=1}^{\infty} \frac{1}{j^2} \ddot{q}_j(\tau) \sin(j\pi\xi) \quad (5)$$

Eq. (6) gives the total bending moment  $M(x, t)$  at beam position  $x$  and time  $t$  as a function of the normalized bending moment  $M(\xi, \tau)$  defined in Eq. (3).

$$M(x, t) = M(\xi, \tau) \sum_{k=1}^2 \left( \sum_{i=1}^5 \frac{P_{ik} L}{4} \right) \quad (6)$$

Eqs. (1) to (6) can then be solved to find the DAFs for mid-span bending moment. The problem can be extended to a series of P-loads moving over a plate model to allow for lateral effects and torsional modes of vibration. In the latter, the meeting of two 5-axle trucks in motion is simulated with a P-load model made of a series of ten loads,  $P_{1k}, P_{2k}, P_{3k}, \dots, P_{10k}$ , deemed to represent the forces exerted by the ten wheels of a truck  $k$  (Fig. 1(b)). The differential equations of motion of the plate model can be expressed in matrix form as in Eq. (7) and solved using a standard integration method such as Runge-Kutta.

$$\mathbf{M}\ddot{\mathbf{v}} + \mathbf{C}\dot{\mathbf{v}} + \mathbf{K}\mathbf{v} = \mathbf{p} \quad (7)$$

where  $\mathbf{p}$  is the forcing vector result of distributing the P-loads to the nodes of the underlying element at each point in time,  $\mathbf{v}, \dot{\mathbf{v}}$  and  $\ddot{\mathbf{v}}$  are the vectors that define the bridge displacements, rotations and their derivatives with respect to time, and  $\mathbf{M}, \mathbf{C}$  and  $\mathbf{K}$  are the mass, damping and stiffness matrixes of the bridge model respectively. In these P-load simulations, it is assumed the mass matrix of the bridge remains constant. This assumption will not be valid for extremely heavy loading events in short span bridges where high vehicle to bridge mass ratios may introduce significant changes in the mass matrix of the system.

## 2.2 Influence of speed and meeting point on DAF

A 25 m span simply supported bridge beam model is used first to illustrate the effect of truck speed on dynamics. The bridge properties are assumed to be those corresponding to a typical beam-and-slab concrete structure carrying two lanes of traffic, i.e., modulus of elasticity  $E = 35 \times 10^9 \text{ N m}^{-2}$ , mass per meter  $\mu = 18360 \text{ kg m}^{-1}$  and second moment of area  $I = 1.39 \text{ m}^4$ . The first natural frequency of the bridge is 4.09 Hz and damping is assumed to be negligible. The static and total midspan bending moments due to crossings of single 5P-load trucks are shown in Fig. 2 for different speeds. For the truck travelling at  $90 \text{ km h}^{-1}$ , the arrivals of the first and second axles at midspan are hardly noticeable while the tridem arrival at midspan denotes a prominent peak with a maximum total moment of 244.2 kN m and a maximum static moment of 227.7 kN leading to a DAF of 1.07. A sharp drop off in moment is evident as the tridem moves away from midspan and towards the end support. This effect is not surprising if it is taken into account that the tridem axles make up almost 60 percent of the total weight. Maximum total moments of 233.1 and 244.5 kN m result into DAFs of 1.02 and 1.07 for vehicle speeds of 70 and  $110 \text{ km h}^{-1}$  respectively.

[FIG. 2 HERE]

Fig. 3(a) shows the results of DAF versus relative position ( $d/L$ ) and frequency ratio (FR) for the case of zero damping and two 5P-load truck models running in opposite directions on a simply supported beam. FR [12] is defined as the ratio of the load circular frequency ( $\pi c/L$ ) to the first circular frequency of the bridge ( $2\pi f_1$ ). If the ‘DAF-FR- $d/L$ ’ relationship was derived for two 1P-loads, DAF would be uniquely defined by these two ratios, FR and  $d/L$ , and it would be valid for all bridges with the same damping, regardless the span length. The pattern of local peaks of DAF in Fig.

3(a) is quite similar to the case of two 1P-loads meeting on a 1D simply supported beam shown by Brady and OBrien [12], in spite of the difference in number of P-loads and axle weight distribution. Each peak corresponds to a matching of effects of bridge natural frequency with the speed and relative spacing of the loads. Speed (proportional to FR) and the parameter  $d$ , can compensate for each other in achieving the time match of constructive/destructive interference that results into these peaks. The amplification of the maximum static response is related to the periodic nature of the dynamic forces, i.e., there are critical speeds that result into bridge inertial forces causing a peak dynamic moment at the same instant the peak static moment takes place. For  $d/L > 0.5$ , the first tridem has passed midspan before the second tridem has reached it, and there is a clear pattern of repeating peaks. Statically, this does not tend to be the most critical case but it is significant in statistical calculations of loading probabilities. For any given speed within this region, the peaks are of equal height as no damping has been considered. When damping is allowed for, the peaks corresponding to  $d$  values in excess of  $0.5L$ , are reduced as might be expected. This is illustrated in Fig. 3(b) for the same bridge, but allowing for 5 percent damping ratio ( $\zeta = 0.05$ ). As in the case of zero damping, there appears to be a pattern of peaks linked in pairs.

[FIG. 3 HERE]

When a single 5-axle truck is modelled using a 10P-load model travelling over one lane of a 2D isotropic plate model, it is possible to evaluate the transverse variation of moments for a given longitudinal section. The longitudinal properties of the plate model are selected to match those of the 1D simulation in Fig. 2. Figs. 4(a) and (b) are

the maximum total and the maximum static moments across the midspan section. Fig. 4(c) is the ‘DAF-speed’ pattern for each transverse location of the midspan section. DAF is obtained dividing the  $z$ -ordinate of Fig. 4(a) by the corresponding ordinate of Fig. 4(b). The critical speeds causing large DAFs at midspan vary between 90 and 105 km h<sup>-1</sup> depending on the transverse location.

[FIG. 4 HERE]

DAF and maximum total moment are also obtained as a function of  $d/L$  and speed when two 10P-load models are driven over different lanes of a 25 m simply supported plate model with a 1.5 percent modal damping. Figs. 5(a) to 5(d) show the DAF and total moment values corresponding to three specific transverse locations within the bridge midspan cross-section, i.e., the bridge centreline and 6 m to the left and to the right of the bridge centreline. The critical static loading cases are those where the two trucks meet near midspan. So, Figs. 5(b), (d) and (f) show that the most important moments develop for  $d/L < 0.5$ . Hence it is reasonable to assume that the peaks of greatest interest are in the range of  $d/L \leq 0.5$ , even although higher DAFs develop outside this region. It can be seen that maximum DAFs are normally associated to small values of total bending moments. In the  $d/L \leq 0.5$  region, there are two important zones: a peak in the interval  $0.2 \leq d/L \leq 0.4$  and FR between 0.14 and 0.16 (A FR of 0.15 is associated to a speed  $c = 2f_1 LFR = 2 \times 4.09 \times 25 \times 0.15 = 30.7$  m s<sup>-1</sup> or 110.4 km h<sup>-1</sup>), and a peak at  $d/L = 0$  corresponding to both tridems meeting at the centre and FR between 0.12 and 0.14 (A FR of 0.13 is associated to 96 km h<sup>-1</sup>). It can be seen that the simplified 1D P-load model of Fig. 1(a) used to generate Fig. 3(a) is sufficient to capture the overall pattern due to a 2D P-load model. There are only

small differences between Figs. 3(a) and 5(a) regarding the level of dynamic amplification and the transverse location under investigation.

[FIG. 5 HERE]

The maximum total moment generally decreases as the transverse location gets closer to the edges of the plate model. It is interesting to observe there is not an identical behaviour in the points symmetrically located with respect to the bridge centreline (Figs 5(a) and 5(e)). For the results of the transverse location in Figs. 5(a) and (b) and for any value of  $d/L$  larger than 0.8 (i.e., both tridems meeting far from the midspan section), there appears to be a constant value of total moment and DAF for a given vehicle speed (or FR), that does not appear in the symmetric transverse location given in Figs. 5(e) and (f). This region of constant values is due to the fact that the maximum total moment will occur when the tridem of the first vehicle is driving over the same lane where the bending moment is being investigated. Nevertheless, the symmetric transverse location will experience maximum moments when the tridem of the second vehicle drives over its side of the cross-section (Figs. 5(e) and (f)), leading to values affected by pre-existing vibrations induced by the first vehicle (only very large values of  $d/L$  could facilitate the bridge to completely damp the vibrations of the first vehicle out). This phenomenon of an initial vibratory condition of a bridge prior to traffic loading has been investigated in detail by Rattigan et al [22].

Fig. 6 illustrates the maximum static bending moment, maximum total bending moment and DAF versus  $d/L$  that has been found within a highway speed range (40 to 120 km h<sup>-1</sup>). Here, DAF has been defined as the maximum total moment divided by

the maximum static moment taking into account seven transverse locations across the midspan section (i.e., at the bridge centreline and at 2, 6 and 7.5 m from the centreline on both sides). The maximum total and maximum static moments may not correspond to the same transverse location. It can be seen the largest moment takes place for  $d/L = 0$ , when both tridems meet at midspan, and the analysis in the following sections will focus on this critical meeting point.

[FIG. 6 HERE]

### 2.3 Influence of bridge length on DAF

To encompass a typical range of designs and to analyse the influence of other axle spacing to span length ratios, two additional spans are considered, 17 m and 35 m, all 15 m wide. The 17 m bridge was assumed to be of beam-and-slab construction, i.e., precast Y-beams with an in-situ slab [23,24],  $\mu = 15000 \text{ kg m}^{-1}$  and  $I = 0.49 \text{ m}^4$  ( $f_1 = 5.82 \text{ Hz}$ ). The 35 m span was assumed to be of similar form but with super-Y beams ( $\mu = 21750 \text{ kg m}^{-1}$ ,  $I = 3.42 \text{ m}^4$ ,  $f_1 = 3.01 \text{ Hz}$ ). Due to the nature of Eq. (1), for a bridge with a given span length and a P-load meeting event with fixed axle spacings and axle weight distribution, the DAF-FR- $d/L$  contour plots are identical regardless the bridge section properties. I.e., if the 17 m bridge was assumed to be of solid construction (precast inverted T-beam with in-situ concrete fill), and the mass per meter and second moment of area were  $\mu = 31875 \text{ kg m}^{-1}$  and  $I = 0.77 \text{ m}^4$  respectively ( $f_1 = 4.99 \text{ Hz}$ ), the DAF-FR- $d/L$  contour plot would be the same as the one given for a 17 m beam-and-slab construction slab. When analyzing DAFs, the critical FR values, as opposed to critical speeds, have the benefit of remaining constant for a given span length. However, the critical speed associated to the dynamic peaks will vary since the



two bridge types have different natural frequencies. I.e., in the 17 m bridge, a typical speed of  $80 \text{ km h}^{-1}$  corresponds to a FRs of 0.112 and 0.131 for the beam-and-slab and solid cross-sections respectively. Beam and isotropic plate models have been built for the 17 m solid slab, and the 17 m, 25 m and 35 m beam-and-slab simply supported bridges. Table 1 shows the values used in the four plate models under investigation. In all plate models, it has been assumed a 1.5 percent modal damping applied to all modes of vibration.

[TABLE 1 HERE]

Figs. 7(a) and (b) show the speeds causing higher DAF for the loading case corresponding to both tridems meeting at the center ( $d/L = 0$ ) and the three bridge spans being analyzed using beam and plate bridge models respectively. Although a 1D beam model is too simple to find DAF directly, here it is shown to give a good approximation of the critical vehicle speeds found in isotropic plate models. Larger differences are expected between both models when allowing for a lower stiffness in the transverse direction than in the longitudinal direction and a higher influence of the transverse modes of vibration. These P-load based simulations can clearly save computational time for a series of more elaborate analyses to be focused on the critical speeds.

[FIG. 7 HERE]

For the case of the 35 m beam model, the maximum DAF is 1.09 and it takes place for  $FR = 0.129$ , corresponding to a critical speed of  $98 \text{ km h}^{-1}$ . The 35 m plate model

gives a maximum DAF of 1.07 for the same FR of 0.129 (98 km h<sup>-1</sup>). The 25 m bridge beam and plate models both have critical FRs of 0.130 which corresponds to a speed of 98 km h<sup>-1</sup> (as result of covering for many possible transverse locations, the plate model also provides a second peak at 105 km h<sup>-1</sup> that it is not as significant in the beam model) and although higher DAFs can be achieved at FR over 0.203 (speeds over 150 km h<sup>-1</sup>), they are unlikely to occur in a critical two-truck meeting event. In the 17 m bridge, both beam and plate bridge models identify an intermediate critical speed at about FR = 0.137. This FR corresponds to a vehicle speed of 84 and 98 km h<sup>-1</sup> for the solid and beam-and-slab cross sections respectively. Then, for the beam model, DAF decreases down to a point of about FR = 0.163, and then DAF increases again reaching at FR = 0.185 (corresponding to vehicle speeds of 113 km/h and 133 km h<sup>-1</sup> for the solid and beam-and-slab cross bridge sections respectively) the same level of DAF as the intermediate critical FR of 0.137. For values of FR higher than 0.185, the pattern shows a continuous increase in DAF in both beam and bridge models, so the speed limit is likely to define one of the critical speeds of the pattern.

While Fig. 7 shows the DAF resulting from taking the maximum total and maximum moment across the plate width regardless its transverse location, Fig. 8 shows ‘DAF-FR’ patterns for two individual transverse locations: the bridge centreline and 6 m from the centreline. The critical speed is sensitive to the transverse location as it was observed for one 5-axle truck (Fig. 4). For both the 25 and 35 m bridges, the critical speeds for the centreline and 6 m from centreline locations are 100 km h<sup>-1</sup> and 94 km h<sup>-1</sup> respectively. In the case of the 17 m bridge, the intermediate critical FR for the centreline is 0.144 (88 km h<sup>-1</sup> if a solid slab or 103 km h<sup>-1</sup> if a beam-and-slab construction) while the other location has an intermediate critical FR of 0.134 (82 km

$\text{h}^{-1}$  and  $96 \text{ km h}^{-1}$  for solid slab and beam-and-slab constructions respectively). For all bridge lengths, there is a difference of about  $6 \text{ km h}^{-1}$  between the critical speeds associated to the two transverse locations.

[FIG. 8 HERE]

## 2.4 Influence of differences in vehicle speeds

For the contour plot of DAF in Fig. 9(a), the meeting point is fixed at  $d/L = 0$  and vehicle speeds are varied for two trucks driving in opposite directions on a two-lane 25 m plate model. The results are symmetric with respect to the  $45^\circ$  line that represents both vehicles travelling at the same speed. Therefore, there is a clear correspondence between a horizontal/vertical section and a section at  $45^\circ$ . The DAF patterns of the first vehicle are shown for fixed speeds of the second vehicle of 55, 70, 85 and  $100 \text{ km h}^{-1}$  in Fig. 9(b). The four patterns are found to be very similar to that pattern of both vehicles travelling at the same speed, with the highest DAFs occurring for the fixed speed of  $100 \text{ km h}^{-1}$ . From Fig. 9(b), it is possible to obtain critical speeds for the first vehicle of 98, 105, 96, and  $98 \text{ km h}^{-1}$ , when the speeds of the second vehicle are fixed to 55, 70, 85 and  $100 \text{ km h}^{-1}$  respectively. These values of critical speeds are very close to the  $98 \text{ km h}^{-1}$  obtained in Fig. 7 using the same speed in both vehicles.

[FIG. 9 HERE]

## 2.5 Influence of the road profile

The response of a 25 m isotropic plate to the crossing of an articulated 5-axle sprung vehicle model allowing for VBI, is used here to test the ability of the P-load model in predicting the critical speeds. The bridge has the mechanical characteristics defined in Table 1. The truck has the same axle spacing and weight distribution used throughout Section 2. The P-loads represent the static weights of the wheels where the paths of the inner and outer wheels are located at 1 and 3 m respectively from the bridge centreline. The ‘DAF-FR’ pattern suggested by the P-loads has been given in Fig. 4(c). Nevertheless, this pattern ignores the variation in dynamic forces caused by the interaction with the road surface and the bridge.

A truck FE dynamic model made of a set of lumped masses, springs and dampers is employed to assess how far the P-load critical speed is from the true critical speed. This vehicle model has 15 independent degrees of freedom: vertical displacement and rotations of the tractor body mass, rotations of the trailer body mass, and the vertical displacements of the 10 axle masses (Fig. 10). A detailed description of the equations of motion governing the response of this mathematical model can be found in Cantero et al [25]. Static axle weights and axle spacings match those defined for the P-load model. A Montecarlo simulation is carried out varying the truck dynamic parameters based on assumed normal distributions for the suspension and tire systems as defined in Table 2 [26-29]. There are two types of suspensions and the values and variability are different for steer, drive and trailer axles. The dynamic interaction between bridge and truck is implemented in Matlab using an iterative procedure described by Green et al [6] and Cantero et al [30]. The iterative procedure has been found in agreement with an alternative VBI procedure based on Lagrange multipliers using

MSc/NASTRAN [11], and it has been preferred because of its flexibility and savings in computational time.

[FIG. 10 HERE]

[TABLE 2 HERE]

The magnitude of the vehicle forces strongly depends on the road unevenness. In this paper, the road profile is assumed to be a random process described by a power spectral density (PSD) function that depends on the road condition and it is implemented using the inverse Fast Fourier Transform as described by Cebon and Newland [31]. The profiles are also passed through a moving average filter to emulate the tyre contact patch [29]. The road condition is characterised by the roughness coefficient  $a$  ( $\text{m}^3\text{cycle}^{-1}$ ) or value of the spectral density at the spatial frequency discontinuity  $\Omega = \frac{1}{2\pi}\text{cycle m}^{-1}$ . Values of the PSD for each spatial natural frequency

( $\Omega$ ) are directly proportional to  $a$  and inversely proportional to  $(2\pi\Omega)^2$  according to ISO specifications [17]. So, the intervals  $a < 8 \times 10^{-6}$  and  $8 \times 10^{-6} \leq a \leq 32 \times 10^{-6}$  fall within ‘very good’ and ‘good’ road classes respectively, which would be expected in well maintained highway surfaces. Fig. 11 illustrates one of the generated random road carpets for a roughness coefficient of  $8 \times 10^{-6} \text{m}^3\text{cycle}^{-1}$ . Each vehicle wheel has a path that is selected from the carpet.

[FIG. 11 HERE]

Profiles with roughness coefficients of  $1 \times 10^{-6}$ ,  $4 \times 10^{-6}$ ,  $8 \times 10^{-6}$ ,  $16 \times 10^{-6}$  and  $32 \times 10^{-6}$

$\text{m}^3\text{cycle}^{-1}$  are used to obtain the bridge response to the single 5-axle truck event. 100 m of approach length are allowed to initially excite the vehicle before entering the bridge. Therefore, 8384 different truck dynamics and road profiles are generated for each roughness coefficient  $a$  (a total of 41920 simulations for all five roughness coefficients being tested). The profile is varied in each simulation by randomly generating the array of numbers defining the phase of each road wavelength. This variation is important because it is not only the height of the road irregularities but also its specific location on the bridge that affect the bridge dynamic response [32]. Figs. 12(a) and (b) show the results of the Monte Carlo simulation for the lowest and higher roughness coefficients respectively. Each point represents the ratio of the maximum total moment to the maximum static moment found at the midspan section. The solid line represents the mean pattern, which has been calculated using a moving average of 100 points. In spite of the variation in road irregularities and truck dynamics, there is a ‘DAF-speed’ pattern. This pattern is clearer for the smooth profile (Fig. 12(a)) that exhibits less scatter than the rough profile of Fig. 12(b)). Fig. 12(b) contains more uncertainty in the level of dynamic amplification due to a strong influence of road roughness and truck dynamics, but if there is sufficient number of points, an underlying mean pattern can still be detected.

[FIG. 12 HERE]

Fig. 13 compares the ‘DAF-speed’ pattern by P-load and the mean ‘DAF-speed’ patterns by sprung models for the five roughness coefficients under investigation. Although the level of dynamic amplification varies, the pattern remains and the critical speeds are only slightly shifted as the roughness coefficient varies. There is

also a widening of the peaks as the road roughness increases. The height and location of the road irregularities will become more important in ‘DAF-speed’ patterns for poor profiles and short bridges. But for the 25 m bridge of Fig. 13, once the roughness coefficient remains below the ‘good’ condition boundary, there is a critical speed of about  $105 \text{ km h}^{-1}$  using sprung models, that can be closely approximated by the P-load model (two peaks in the P-load pattern with critical speeds of  $99 \text{ km h}^{-1}$  and  $105 \text{ km h}^{-1}$ ). It must be noted the similarities between the ‘DAF-speed’ patterns predicted by a P-load model for a single 5-axle truck (Fig. 13) and for a two 5-axle truck meeting event with  $d/L = 0$  (Fig. 7(b)). As the road profile gets poorer and the bridge span gets shorter, it is expected that the P-load model will gradually lose accuracy in the prediction of a pattern that will become governed by the road profile. Deng and Cai [33] investigated the dynamic amplification due to the crossing of an AASHTO HS20-44 truck travelling over multi-girder concrete bridges for seven speeds between 30 and 120 km/h, five span lengths between 9.14 and 39.62 m, and ISO road classes varying from ‘very good’ to ‘very poor’ condition. They showed graphs of impact factors versus speed where patterns can also be identified. It can be seen how these patterns were altered by road roughness, and how the differences appeared to be more significant for shorter bridge spans.

[FIG. 13 HERE]

Fig. 14 shows the bending moments at the midspan bridge centreline for a critical speed of  $105 \text{ km h}^{-1}$  due to the P-load model and to a random sprung model on the road carpet of Fig. 11. This figure illustrates why the P-load model is able to predict the pattern found in more complex VBI models with a ‘good’ road profile. The total

moment by both models oscillate around the bridge static response. These dynamic oscillations may have different amplitudes depending on the road roughness and dynamic characteristics of the vehicle, but for a given vehicle speed, the peaks of the oscillations hardly vary their location with respect to the location of the maximum static. As result, the P-load model is able to identify the speeds when the maximum dynamic peak develops over the location of the maximum static moment with the potential of leading to a large DAF.

[FIG. 14 HERE]

### **3. Experimental testing**

Strain measurements due to the passage of traffic have been collected in a bridge located in Vranks, Slovenia, during the ARCHES project [18]. SiWIM [19] has been employed to provide vehicle speed, number of axles, weights and axle spacings for each traffic event using the strain measured under the bridge soffit. This modern Bridge Weigh-In-Motion system can also estimate the maximum static strain using a low-pass filter that removes the dynamic component of the measured strain. The ratio between maximum measured strain and maximum static strain gives a value of DAF for the crossing of each vehicle that can be used to obtain the mean ‘DAF-speed’ pattern of a particular truck population.

#### *3.1 Field measurements*

The bridge is a two-lane simply supported structure with traffic in opposite directions and 24.8 m span length. Single events of two modes of a 2-axle rigid truck population



were selected for monitoring of their DAF and speed because of its high number of occurrences on the Vransko site. A total of 7603 and 8913 2-axle trucks were recorded for the light and heavy modes respectively between the 25<sup>th</sup> September 2006 and the 21<sup>st</sup> November 2006. Mean and standard values for axle spacings and weights are defined in Table 3.

[TABLE 3 HERE]

Fig. 15 shows the histograms of speed for the two truck modes under investigation. As expected, lighter vehicles tend to travel faster as shown by the higher number of occurrences of mode 1 over mode 2 between 100 and 120 km h<sup>-1</sup>.

[FIG. 15 HERE]

The road profile was measured with the ZAG-VP longitudinal profilometer [18]. Measurements were performed on the normal right wheel path in each lane. They started 80 m before the bridge and were extended for 80 m after leaving the bridge. The 150 m IRI (International Roughness Index) index is typically used to assess roughness of the pavement on the network level and IRI<sub>150</sub> of 2.96 and 2.04 mm m<sup>-1</sup> were obtained for the right and left lanes respectively. While simulations normally generate relatively “uniformly uneven” road profiles, the measured road profiles address the major unevennesses that often occur around the expansions joints, either due to their damage or due to the settlements of the pavement just before or after the bridge. Experiences show that the residual displacements of soil near the bridge can often, in the first years after the bridge construction, initiate bumps that increase the

DAF values. These were observed on the 10-year old Vransko bridge, particularly in the right lane (Fig. 16(a)). However, due to the length of the section,  $IRI_{150}$  filters out the bumps and other major unevennesses around and on the bridge that excite the bridge response and, as a result, increase the DAF values. Thus, IRI indices were also calculated on shorter sections, i.e., over 20 meter sections ( $IRI_{20}$ ) and over 10 meter sections ( $IRI_{10}$ ) to illustrate the local conditions. Fig. 16 shows the measured profiles and the calculated values of  $IRI_{20}$  and  $IRI_{10}$  for each lane. . The bridge has not been resurfaced since it was constructed and it has values of  $IRI_{20} = 3.30$  and  $IRI_{10} = 5.20 \text{ mm m}^{-1}$  in the right lane of the bridge, and  $IRI_{20} = 2.20$  and  $IRI_{10} = 2.83 \text{ mm m}^{-1}$  in the left lane (equivalent to a roughness coefficient  $a$  below  $32 \times 10^{-6} \text{ m}^3 \text{ cycle}^{-1}$ ). These IRI values fall within the range of ‘good’ road profiles investigated in the Section 2.5.

[FIG. 16 HERE]

The points in Fig. 17 represent all the measured DAFs. The figure also shows the mean ‘DAF-speed’ pattern, which is obtained from averaging every  $10 \text{ km h}^{-1}$  while progressing in steps of  $2 \text{ km h}^{-1}$ .

[FIG. 17 HERE]

It would be expected to have a better definition of the pattern in those speed regions where there is a more dense truck population (i.e., between  $80$  and  $90 \text{ km h}^{-1}$  according to histogram of Fig. 15). Fig. 18 compares both modes for three sample sizes: the full sample size, and the first  $2/3$  and  $1/3$  of the sample entering the bridge.

It can be seen how the pattern converges faster towards the pattern of the full sample in those intermediate speed regions with many truck occurrences. It is evident a minimum number of trucks is needed to characterise the mean ‘DAF-speed’ pattern of a given sample and an extended measurement period would be needed to characterize the least frequent lower and upper speed ranges. It can also be observed there are only small differences in the ‘DAF-speed’ pattern of both truck modes.

[FIG. 18 HERE]

### *3.2 Theoretical and experimental critical speeds*

The mean values for axle spacing and axle weights from Table 3 are used as parameters for a 4P-load vehicle model representing the 4 wheels of a 2-axle rigid truck. An orthotropic bridge plate model is built based on the experimentally validated FEM of the Vransko bridge described by Cillian et al [34]. The longitudinal and transverse moduli of elasticity of the bridge model are  $3.5 \times 10^{10}$  and  $1.4 \times 10^{10}$  N m<sup>-2</sup> respectively, and the first longitudinal and transverse modes of vibration have frequencies of 5.32 Hz and 13.76 Hz respectively. Numerical simulations of the bridge response of the Vransko bridge model to moving P-loads are used to predict the critical speeds associated to the 2-axle truck using Eq. (7). The patterns due to the P-load model associated to the 2 modes under investigation are compared to those found experimentally in Fig. 19. For the heavy 2-axle truck mode, the P-load model correctly estimates the maximum critical speed in 87 km h<sup>-1</sup>, while for the light mode there is a small discrepancy with the P-load model giving a critical speed of 86 km h<sup>-1</sup> compared to the measured 89 km h<sup>-1</sup>. Other features of the pattern are recognised in the theoretical model, i.e., both experimental and theoretical patterns have a higher trough to the left of the central peak than the trough to the right of the DAF peak.

[FIG. 19 HERE]

The dynamic patterns of both truck modes are very similar but they appear slightly shifted with speed. The direction of the shift differs in the theoretical and experimental patterns. It must be noted that the population of the light truck mode is smaller than the heavy mode, and the measured mean pattern may not be as reliable as for the heavy mode. Therefore, there will generally appear differences between the measured and predicted pattern to some extent as a result of a limited sample size within some speed ranges, relatively large standard deviations of gross weights and their distribution (there will be a different ‘DAF-speed’ response for each specific vehicle), the road roughness, variations in the lateral position of the vehicle or discrepancies between the mathematical bridge model and reality. Nevertheless, it has been shown that a simulation model based on P-loads is a valuable tool to approximate the location of peaks and troughs found in an experimental pattern.

#### **4. Conclusions**

When simulating the dynamic interaction between a vehicle and a bridge, there are many uncertainties involving parameters of difficult estimation on the field. A model consisting of a series of moving constant point loads (P-loads) has been employed here to identify the critical speeds that place the bridge under highest total moment. This simple model only takes into account bridge dynamics, but if the road profile was relatively smooth, it can be used to predict the worst speed scenarios derived from complex VBI models or from bridge measurements.

The values and spacings of the P-loads must be adjusted to be in agreement with the static weights and spacings of the vehicles being modeled. Contour plots of maximum dynamic amplification versus frequency ratio and normalized relative distance between trucks have been obtained using simulations of P-loads over two types of bridge models: a 1D beam and a 2D FE isotropic plate. 2D/3D bridge models are necessary to allow for the effect of the transverse position of the vehicle and to analyse the load effect at different transverse locations across the width. Nevertheless, it has been shown that a 1D beam model may provide a first approximation of the critical speeds. Critical meeting events of typical 5-axle trucks travelling in opposite directions have been simulated over four medium-span bridges. Truck speeds have been varied resulting into contour plots that reveal a clear pattern consisting of a series of dynamic peaks and troughs associated to different speeds and distances between trucks. As speed increases, the peaks tend to be wider and higher, i.e., more significant dynamics. This trend is limited by the maximum speeds to be expected on a motorway, and so, four main critical peak speeds have been identified within a motorway speed range. If a frequency ratio parameter relating vehicle speed and bridge frequency was employed, the resulting 'DAF-FR' pattern is found to be less sensitive to changes in span length than the 'DAF-speed' pattern. Therefore, for a given span length and traffic event, the critical speed will vary with the properties of the cross-sectional bridge, but the critical FR relating vehicle speed and bridge natural frequency will remain the same.

Then, the critical speeds have been obtained for a more realistic scenario using complex spring-dashpot truck models and allowing for interaction with the road and

the bridge. The bridge has been idealised as an isotropic plate model. The 5-axle vehicle has been modelled as a 15 degree-of-freedom model consisting of mass, rigid and spring elements. Truck dynamic properties have been varied using MonteCarlo simulation, and road carpets have been randomly generated using power spectral density functions as defined by ISO standards. A large sample of ‘very good’ and ‘good’ ISO road profiles have been used to derive their associated ‘DAF-speed’ patterns. In order to compare results from the VBI model to the P-load approach, allowance has been made for accurate transverse location of the P-load model on the bridge. It has been shown that for medium-span bridges, the P-load model can predict the number of peaks and troughs in the pattern and those critical speeds once the spatial geometric mean remains within ‘very good’ and ‘good’ road classes. The smoother the profile, the more accurate the predicted ‘DAF-speed’ pattern becomes. For traffic events made of other vehicle configurations, the values and spacings of the P-loads will need to be readjusted and the number of peaks and their location will clearly be different.

Finally, a field trial has been carried out on a bridge in Slovenia with the aim of comparing the critical speeds that a P-load model would suggest to those measured on site. Maximum total strain, static strain, vehicle speed, weights and axle spacings have been collected using Bridge Weigh-In-Motion technology. This data has been used to obtain the experimental ‘DAF-speed’ patterns for two 2-axle truck populations. Then, a theoretical FE plate model of the bridge has been built based on bridge drawings and measurements, and a 4P-load model has been defined for each vehicle population based on the average measured wheel static weights and axle spacings. It has been

shown how the experimental critical speeds have compared well with those peaks in the theoretical ‘DAF-speed’ pattern using a simple P-load model.

## **Acknowledgments**

The authors would like to express their gratitude for the support received from the 6th European Framework Project ARCHES (2006-09) towards this investigation.

## **References**

- [1] N.J. Ricketts, J. Page, Traffic data for highway bridge loading, Transport Research Laboratory, TRL Report 251, 1997.
- [2] S. Grave, Modelling of site-specific traffic loading on short to medium span bridges, PhD Thesis, Department of Civil Engineering, Trinity College, Dublin, Ireland, 2001.
- [3] S.P. Brady, E.J. O'Brien, A. Žnidarič, The effect of vehicle velocity on the dynamic amplification of a vehicle crossing a simply supported bridge, *ASCE Journal of Bridge Engineering* 11(2) (2006) 241-249.
- [4] DIVINE Programme, Dynamic interaction of heavy vehicles with roads and bridges. DIVINE Concluding Conference, Ottawa, Canada, June, 1997.
- [5] A. Greco, A. Santini, Dynamic response of a flexural non-classically damped continuous beam under moving loadings, *Computers and Structures* 80 (2002) 1945-1953.
- [6] M.F. Green, D. Cebon, D.J. Cole, Effects of vehicle suspension design on dynamics of highway bridges, *ASCE Journal of Structural Engineering* 121(2) (1995) 272-282.

- [7] M. Fafard, M. Bennur, M. Savard, A general multi-axle vehicle model to study the bridge-vehicle interaction, *Engineering Computations* 15(5) (1997) 491-508.
- [8] C. Liu, D. Huang, T.L. Wang, Analytical dynamic impact study based on correlated road roughness, *Computers and Structures* 80 (2002) 1639-1650.
- [9] M. Olsson, On the fundamental moving load problem, *Journal of Sound and Vibration* 154(2) (1991) 299-307.
- [10] D. McLean, M.L. Marsh, Dynamic impact factors for bridges, NCHRP synthesis 266, Transportation Research Board, National Research Council, 1998.
- [11] A. González, P. Rattigan, E. O'Brien, C. Caprani, Determination of bridge lifetime DAF using finite element analysis of critical loading scenarios, *Engineering Structures* 30(9) (2008) 2330-2337.
- [12] S.P. Brady, E.J. O'Brien, The effect of vehicle velocity on the dynamic amplification of two vehicles crossing a simply supported bridge, *ASCE Journal of Bridge Engineering* 11(2) (2006) 250-256.
- [13] J.L. Humar, A.H. Kashif, Dynamic response analysis of slab-type bridges, *ASCE Journal of Structural Engineering* 121(1) (1995) 48-62.
- [14] P.H. Kirkegaard, S.R.K. Nielsen, I. Enevoldsen, Heavy vehicles on minor highway bridges – Calculation of dynamic impact factors from selected crossing scenarios. Paper No. 172, Dept. of Building Technology and Structural Engineering, Aalborg University, Aalborg, Denmark, ISBN 1395-7953 R9722, 1997.
- [15] Y.B. Yang, S.S. Liao, B.H. Lin, Impact formulas for vehicles moving over simple and continuous beams, *ASCE Journal of Structural Engineering* 121(11) (1995) 1644-1650.
- [16] X.Q. Zhu, S.S. Law, Dynamic load on continuous multi-lane bridge deck from moving vehicles, *Journal of Sound and Vibration* 251(4) (2002) 697-716.



- [17] International Organization for Standardization ISO 8608, Mechanical vibration - road surface profiles - reporting of measured data, 1995.
- [18] ARCHES Programme, Assessment and rehabilitation of central European Highway Structures. WP 2: Structural Assessment and Monitoring, EU 6<sup>th</sup> Framework, 2006-2009. <http://arches.fehrl.org/>. Accessed December 9, 2009.
- [19] A. Žnidarič, I. Lavrič, J. Kalin, Measurements of bridge dynamics with a bridge weigh-in-motion system, *Proceedings of the Fifth International Conference on Weigh-In-Motion*, Jacob B, Obrien E.J., O'Connor A., Bouteldja M Eds, ISTE Publishers, Paris, France, 2008, pp. 388-397.
- [20] The Mathworks, Inc., Using MATLAB, Version 6, USA, 2003. <http://www.mathworks.com>
- [21] L. Frýba, *Vibration of Solids and Structures under Moving Loads*, Noordhoff International Publishing, Groningen, The Netherlands, 1972, re-issued 1999.
- [22] P. Rattigan, A. González, E. O'Brien, The influence of pre-existing vibrations on the dynamic response of medium-span bridges, *Canadian Journal of Civil Engineering* 36(1) (2009) 73-74.
- [23] H.P.J. Taylor, L.A. Clark, C.C. Banks, The Y-beam: a replacement for the M-beam in beam-and-slab bridge decks, *The Structural Engineer* 68 (23) (1990) 459-465.
- [24] H.P.J. Taylor, The precast concrete bridge beam: the first 50 years, *The Structural Engineer* 76 (21) (1998) 407-414.
- [25] D. Cantero, E.J. OBrien, A. González, Modelling the vehicle in vehicle-infrastructure dynamic interaction studies, *Proceedings of the Institution of Mechanical Engineers, Part K, Journal of Multi-body Dynamics* 224 (2010) 459-465. doi: 10.1243/14644193JMBD228
- [26] J.Y. Wong, *Theory of Ground Vehicles*, John Wiley & Sons, 1993.

- [27] T.T. Fu, D. Cebon, Analysis of a truck suspension database, *International Journal of Heavy Vehicle Systems* 9:4 (2002) 281-297.
- [28] P.H. Kirkegaard, S.R.K. Nielsen, I. Enevoldsen, Heavy vehicles on minor highway bridges – Dynamic modelling of vehicles and bridges. Report in Department of Building technology and Structural Engineering, Aalborg University, ISSN 1395-7953 R9721, December, 1997.
- [29] N.K. Harris, E.J. O'Brien, A. González, Reduction of bridge dynamic amplification through adjustment of vehicle suspension damping, *Journal of Sound and Vibration* 302:3 (2007) 471-485.
- [30] D. Cantero, E.J. O'Brien, A. González, B. Enright, C. Rowley, Highway bridge assessment for dynamic interaction with critical vehicles, *10th International Conference on Safety, Reliability and Risk of Structures, ICOSSAR 2009*, Furuta, Frangopol & Shinozuka, Taylor & Francis eds, Osaka, Japan, 2009, pp. 3104-3109.
- [31] D. Cebon, D.E. Newland, Artificial generation of road surface topography by the inverse F.F.T. method, *Vehicle System Dynamics* 12:1 (1983) 160-165. doi: 10.1080/00423118308968747
- [32] Y.Y. Li, E.J. O'Brien, A. González, The development of a dynamic amplification estimator for bridges with good road profiles, *Journal of Sound and Vibration* 293:1-2 (2006) 125-137.
- [33] L. Deng, C.S. Cai, Development of dynamic impact factor for performance evaluation of existing multi-girder concrete bridges, *Engineering Structures* 32 (2010) 21-31.
- [34] C.W. Rowley, E.J. O'Brien, A. González, A. Žnidarič, Experimental testing of a moving force identification bridge weigh-in-motion algorithm, *Experimental Mechanics* 49:5 (2009) 743-746. doi: 10.1007/s11340-008-9188-3

Fig. 1 – Simple P-load simulation of two 5-axle vehicles travelling in opposite directions: (a) beam model, (b) plate model.

Fig. 2 – Midspan bending moment due to a single 5P-load truck crossing a beam model at different speeds: static (solid line), 70 (dotted line), 90 (dashed-dotted line) and 110 (dashed line)  $\text{km h}^{-1}$ .

Fig. 3 – Dynamic amplification factor due to two 5P-load trucks meeting on a 25 m beam model: (a) zero damping, (b) 5 percent damping.

Fig. 4 – Bridge response at midspan due to a single 10P-load truck crossing a plate model: (a) total moment (kN m) - transverse location - speed, (b) static moment - transverse location, (c) DAF - speed - transverse location.

Fig. 5 – Transverse variation of DAF and total moment (kN m) within the midspan cross-section: (a) ‘DAF- $d/L$ -FR’ at 6 m to the left of the bridge centreline, (b) ‘Maximum total moment - $d/L$ -FR’ at 6 m to the left of the bridge centreline, (c) ‘DAF- $d/L$ -FR’ at the bridge centreline, (d) Maximum total moment - $d/L$ -FR’ at the bridge centreline, (e) ‘DAF- $d/L$ -FR’ at 6 m to the right of the bridge centreline, (f) Maximum total moment - $d/L$ -FR’ at 6 m to the right of the bridge centreline.

Fig. 6 - Maximum static bending moment (dotted line), maximum total bending moment (solid line) and DAF (dashed line) values at midspan versus  $d/L$  for a meeting event on a 25 m plate model.

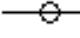
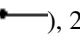
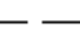
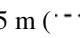
Fig. 7 – Dynamic amplification factor versus frequency ratio for 17 m solid slab (  ), and 17 m (  ), 25 m (  ) and 35 m (  ) beam-and-slab bridges: (a) two 5P-loads meeting on a beam model, (b) two 10P-loads meeting on a plate model.

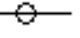
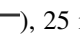
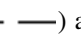
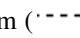
Fig. 8 – Dynamic amplification factors for midspan of 17 m solid slab (  ), and 17 m (  ), 25 m (  ) and 35 m (  ) beam-and-slab bridges: (a) bridge centreline; (b) 6 m from bridge centreline.

Fig. 9 – Dynamic amplification factor due to vehicles travelling at different speeds: (a) contour plot of DAF versus combinations of vehicle speeds, (b) sections for speeds of the second vehicle of 55 (dashed line), 70 (dotted line), 85 (dashed-dotted line) and 100 (solid line)  $\text{km h}^{-1}$ .

Fig. 10 – Sprung vehicle model: (a) side view, (b) front view.

Fig. 11 – Road profile carpet.

Fig. 12 – Individual outputs (dots) and mean pattern (solid line) resulting from Montecarlo simulation for two roughness coefficients: (a)  $a = 1 \times 10^{-6} \text{ m}^3 \text{ cycle}^{-1}$ , (b)  $a = 32 \times 10^{-6} \text{ m}^3 \text{ cycle}^{-1}$ .

Fig. 13 – ‘DAF-speed’ pattern by P-load model (—\*—) and mean ‘DAF-speed’ pattern by VBI model for a variety of road roughness:  $a = 1 \times 10^{-6}$  (—),  $a = 4 \times 10^{-6}$  (---),  $a = 8 \times 10^{-6}$  (—),  $a = 16 \times 10^{-6}$  (—) and  $a = 32 \times 10^{-6}$  (—)  $\text{m}^3 \text{ cycle}^{-1}$ .

Fig. 14 – Midspan static and total bending moments due to 5-axle truck event modelled as 10P-loads and as a sprung model: static (dashed line), total due to P-loads (solid line) and total due to VBI model (dotted line).

Figure 15 – Speed histogram for 2-axle truck population: 1<sup>st</sup> mode (■), 2<sup>nd</sup> mode (□).

Figure 16 – Measured longitudinal road profile (—), IRI 10m (.....), IRI 20m (---) and location of the bridge (■): (a) right lane, (b) left lane.

Figure 17 – Measured DAF (o) and mean ‘DAF-speed’ pattern (—\*—) for 2-axle trucks: (a) 1<sup>st</sup> mode, (b) 2<sup>nd</sup> mode.

Figure 18 – Influence of the sample size on the pattern: full sample of 1<sup>st</sup> mode (—Δ—), 2/3 of 1<sup>st</sup> mode sample (---Δ---), 1/3 of 1<sup>st</sup> mode sample (---Δ---), full sample of 2<sup>nd</sup> mode (—Δ—), 2/3 of 2<sup>nd</sup> mode sample (---Δ---) and 1/3 of 2<sup>nd</sup> mode sample (---Δ---).

Figure 19 – ‘DAF-speed’ patterns: theoretical 1<sup>st</sup> mode (---), theoretical 2<sup>nd</sup> mode (—), experimental 1<sup>st</sup> mode (---Δ---) and experimental 2<sup>nd</sup> mode (—\*—).

Table 1 Characteristics of the bridge plate models

Table 2 Parameters of 5-axle truck simulation

Table 3 Weigh-In-Motion data on 2-axle truck population

Table 1

span (m)	depth (m)	density (kg m <sup>-3</sup> )	1 <sup>st</sup> frequency (Hz)		damping ratio(%)	Young's mod. (N m <sup>-2</sup> )	Poisson's ratio	width (m)
			longit.	transv.				
17 <sup>a</sup>	0.845	2515	4.99	9.36	1.5	3.5x10 <sup>10</sup>	0.2	15
17 <sup>b</sup>	0.730	1370	5.84	10.97	1.5	3.5x10 <sup>10</sup>	0.2	15
25 <sup>b</sup>	1.032	1186	4.09	10.44	1.5	3.5x10 <sup>10</sup>	0.2	15
35 <sup>b</sup>	1.396	1039	3.01	10.35	1.5	3.5x10 <sup>10</sup>	0.2	15

<sup>a</sup>solid slab construction, <sup>b</sup>beam-and-slab construction

Table 2

	<b>Units</b>	<b>Mean</b>	<b>St. Deviation</b>	<b>Minimum</b>	<b>Maximum</b>
Steer suspension stiffness	N m <sup>-1</sup>	3x10 <sup>5</sup>	0.7x10 <sup>5</sup>	1.5x10 <sup>5</sup>	5x10 <sup>5</sup>
Drive suspension stiffness (air)	N m <sup>-1</sup>	5x10 <sup>5</sup>	0.5x10 <sup>5</sup>	3x10 <sup>5</sup>	6x10 <sup>5</sup>
Drive suspension stiffness (steel)	N m <sup>-1</sup>	10x10 <sup>5</sup>	3x10 <sup>5</sup>	6x10 <sup>5</sup>	15x10 <sup>5</sup>
Trailer suspension stiffness (air)	N m <sup>-1</sup>	4 x10 <sup>5</sup>	1x10 <sup>5</sup>	2.5x10 <sup>5</sup>	6x10 <sup>5</sup>
Trailer suspension stiffness (steel)	N m <sup>-1</sup>	12.5x10 <sup>5</sup>	2x10 <sup>5</sup>	10x10 <sup>5</sup>	15x10 <sup>5</sup>
Suspension viscous damping	N s m <sup>-1</sup>	5x10 <sup>3</sup>	2x10 <sup>3</sup>	3x10 <sup>3</sup>	10x10 <sup>3</sup>
Tyre stiffness	N m <sup>-1</sup>	7.5x10 <sup>5</sup>	2x10 <sup>5</sup>	5x10 <sup>5</sup>	1.5x10 <sup>5</sup>
Tyre damping	N s m <sup>-1</sup>	3x10 <sup>3</sup>	1x10 <sup>3</sup>	2x10 <sup>3</sup>	10x10 <sup>3</sup>
Fifth wheel distance	m	0.65	0.1	0.5	1.3
Suspension offset (steer and trailer axles)	m	0.1	0.05	0.08	0.3
Suspension offset (drive axle)	m	0.5	0.05	0.35	0.6
Speed	km h <sup>-1</sup>	80.5	12.6	60	120

Table 3

Mode	Gross Weight (kN)		Axle spacing (m)		Front axle (kN)		Rear axle (kN)	
	Mean	St.Dev.	Mean	St. Dev.	Mean	St.Dev.	Mean	St.Dev.
1 <sup>st</sup>	59.05	9.29	4.27	0.58	25.34	6.38	33.71	7.85
2 <sup>nd</sup>	117.53	20.68	4.81	0.73	40.99	10.17	76.54	18.32

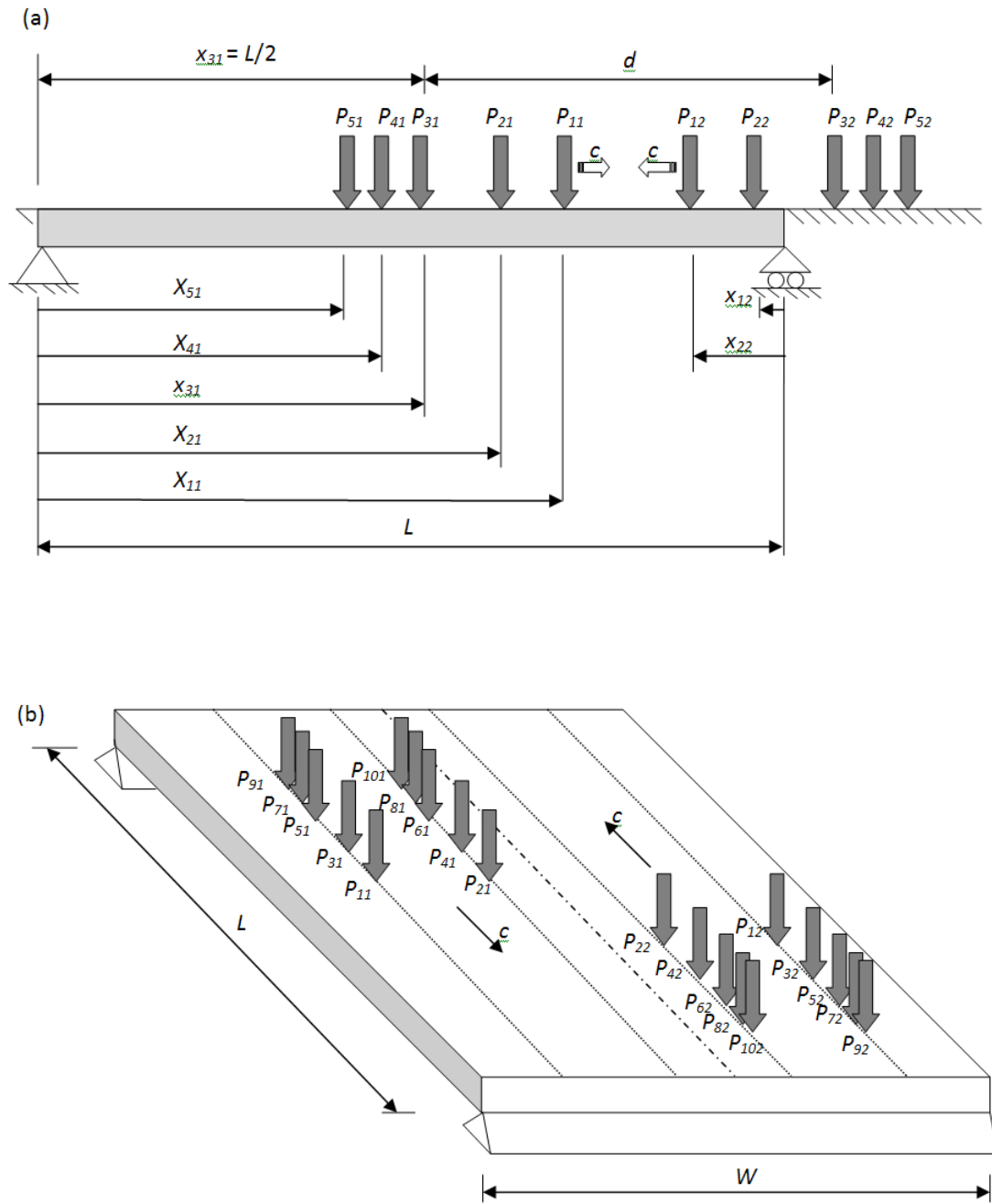


Figure 1



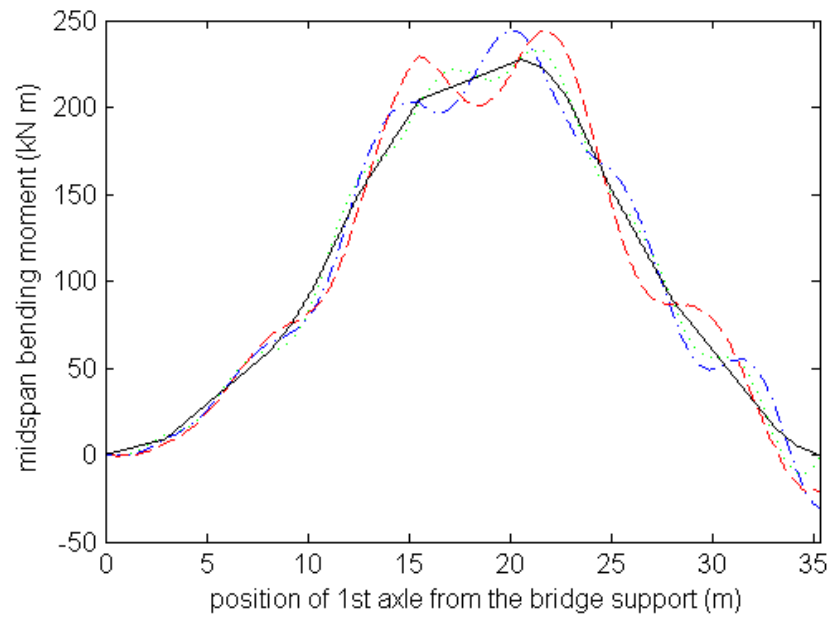


Figure 2

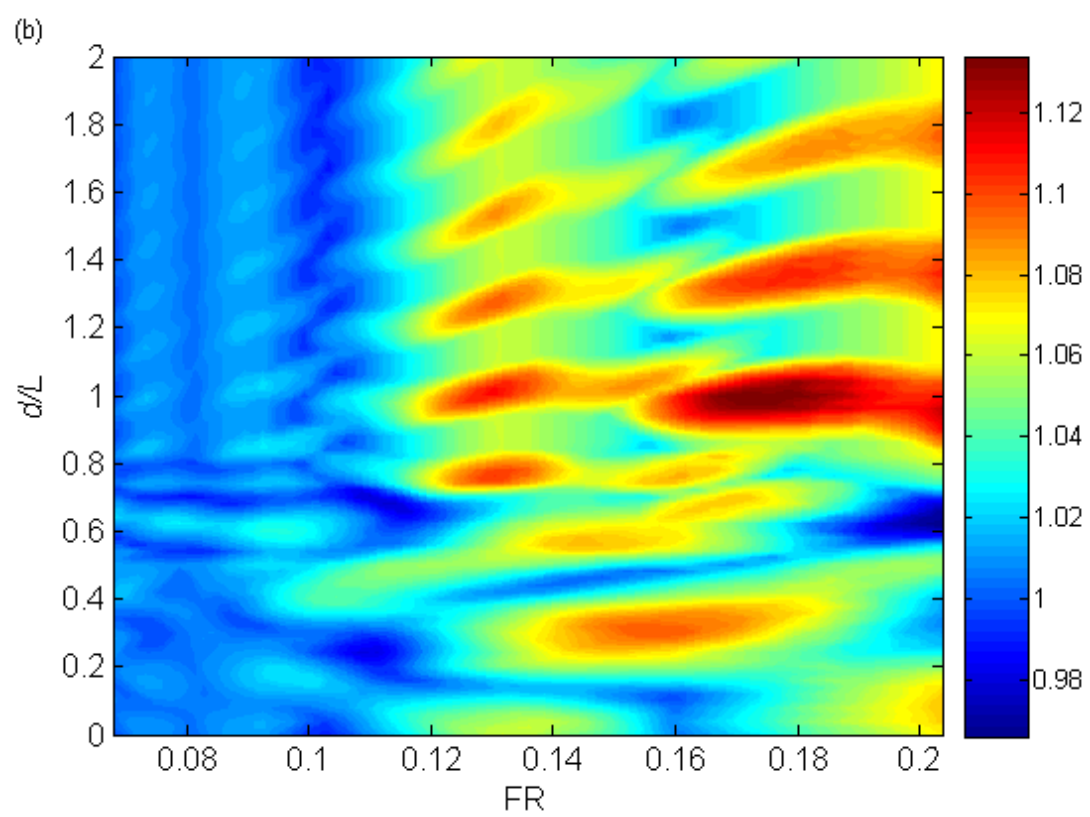
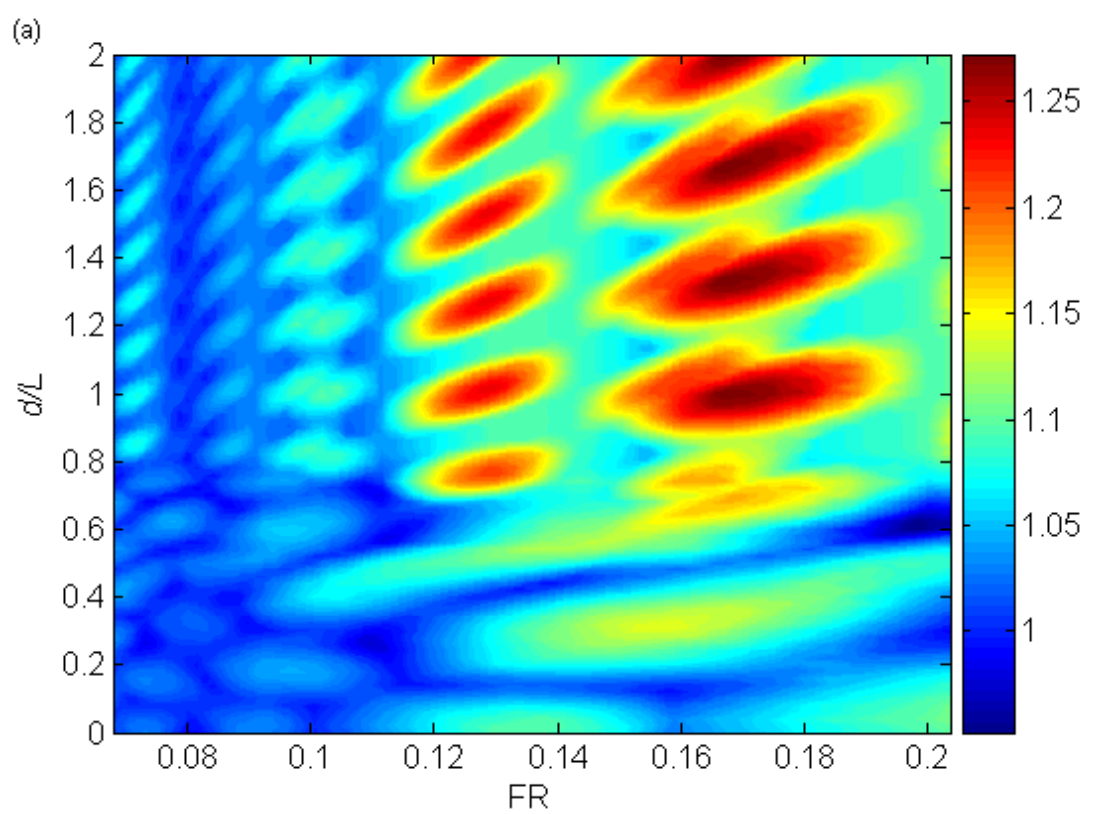


Figure 3

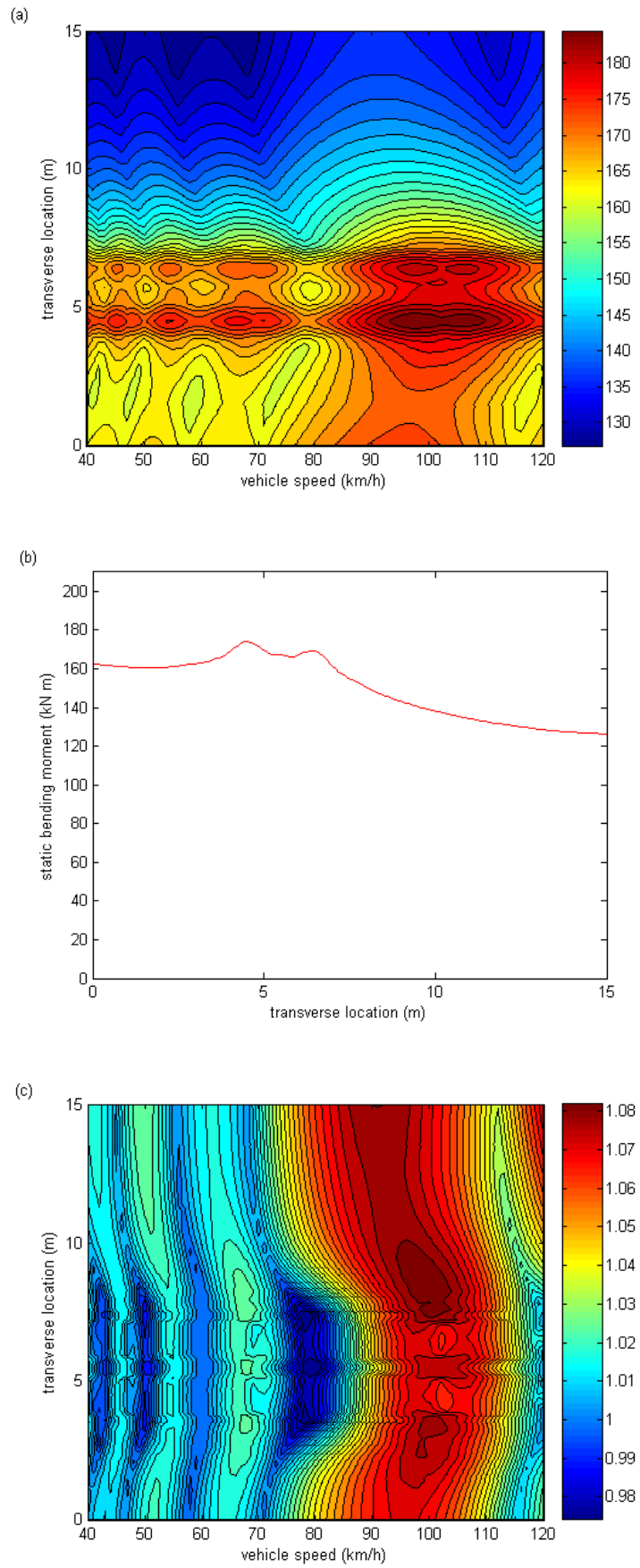


Figure 4



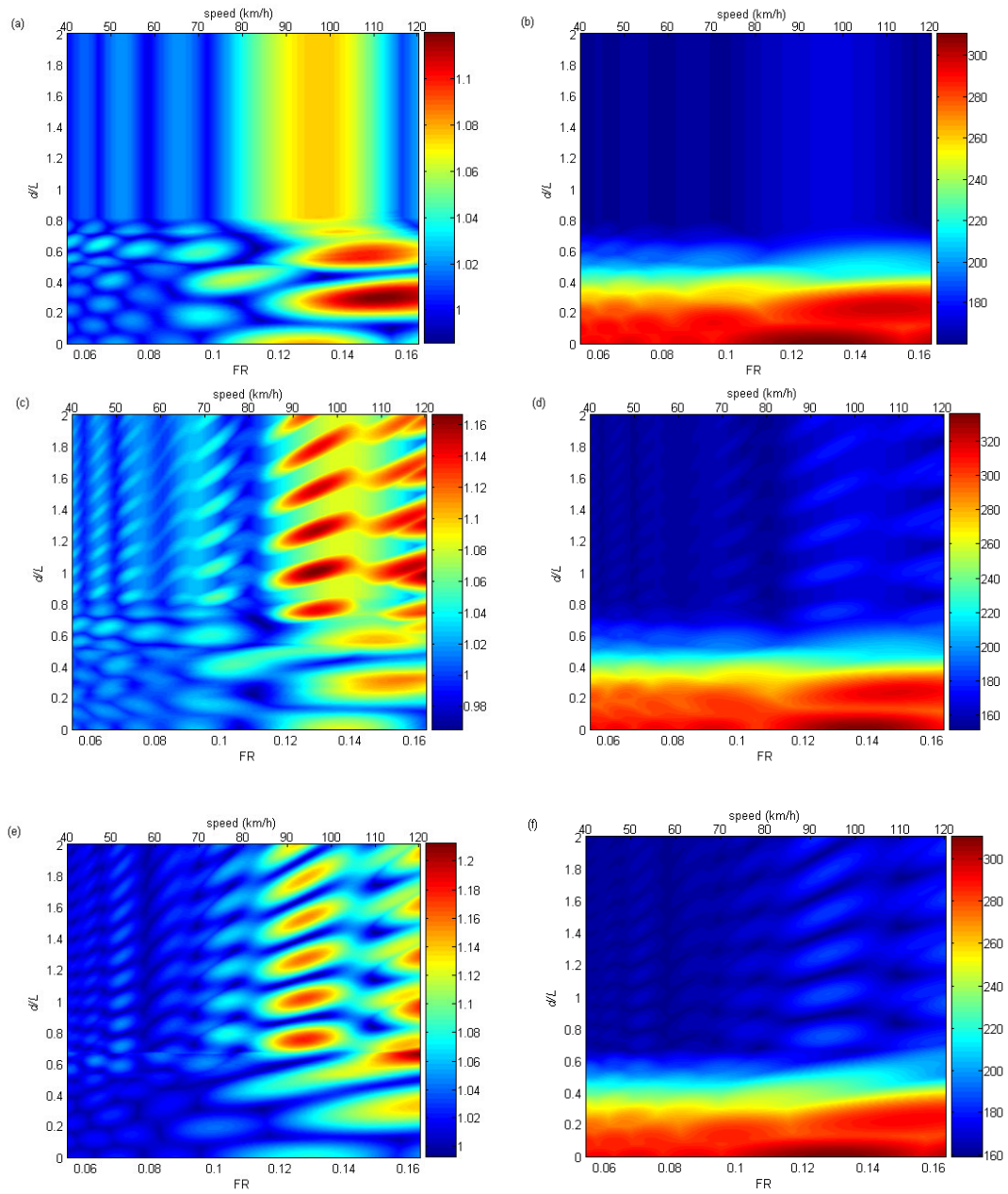


Figure 5

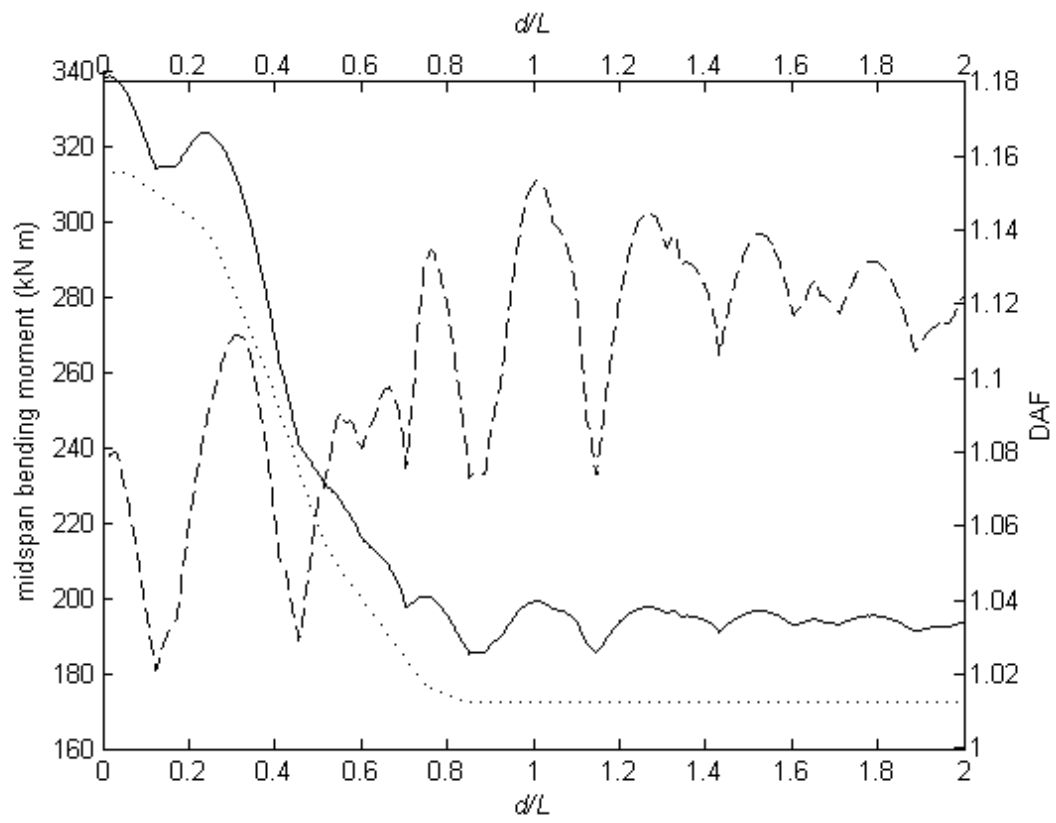


Figure 6

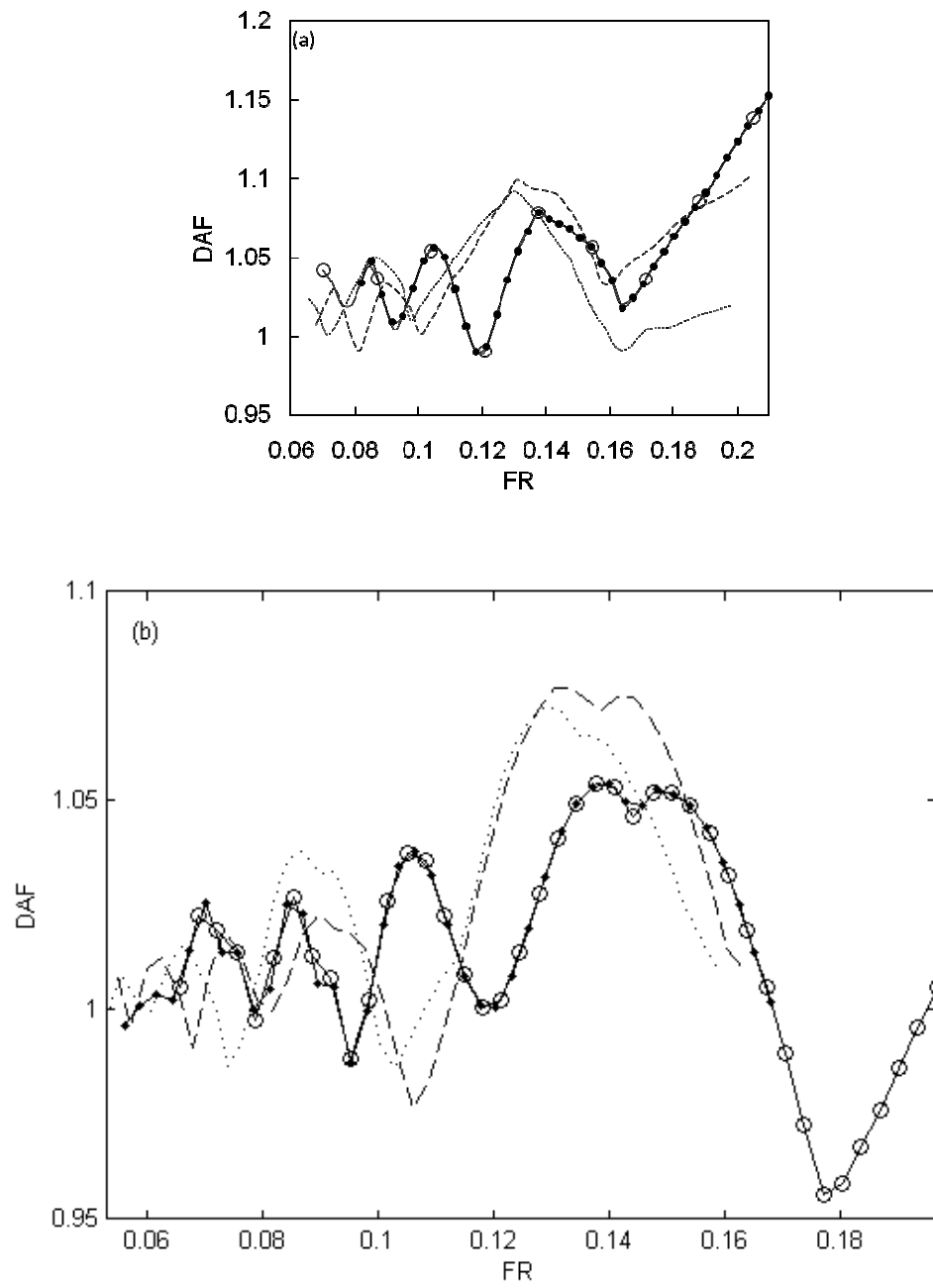


Figure 7

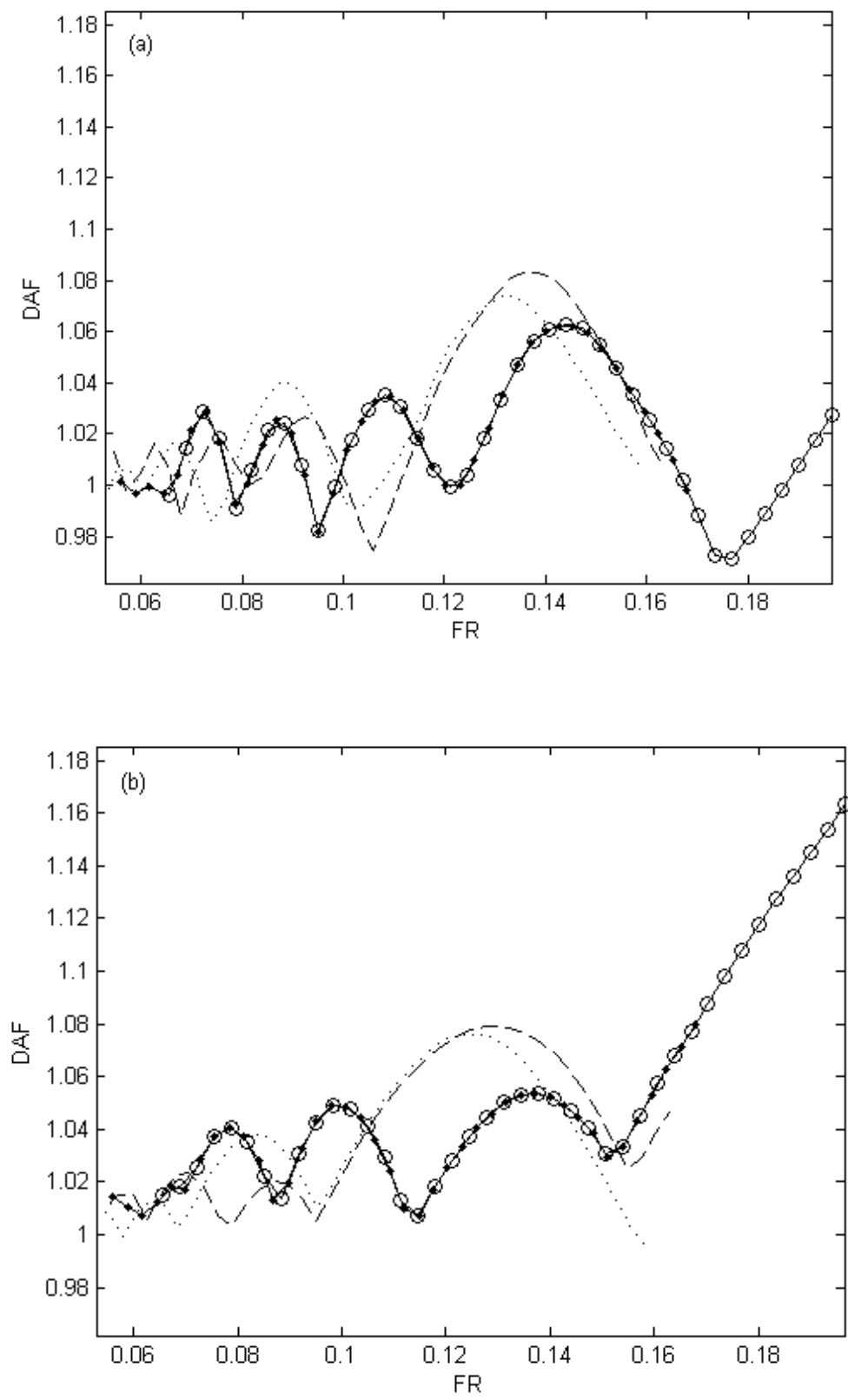


Figure 8



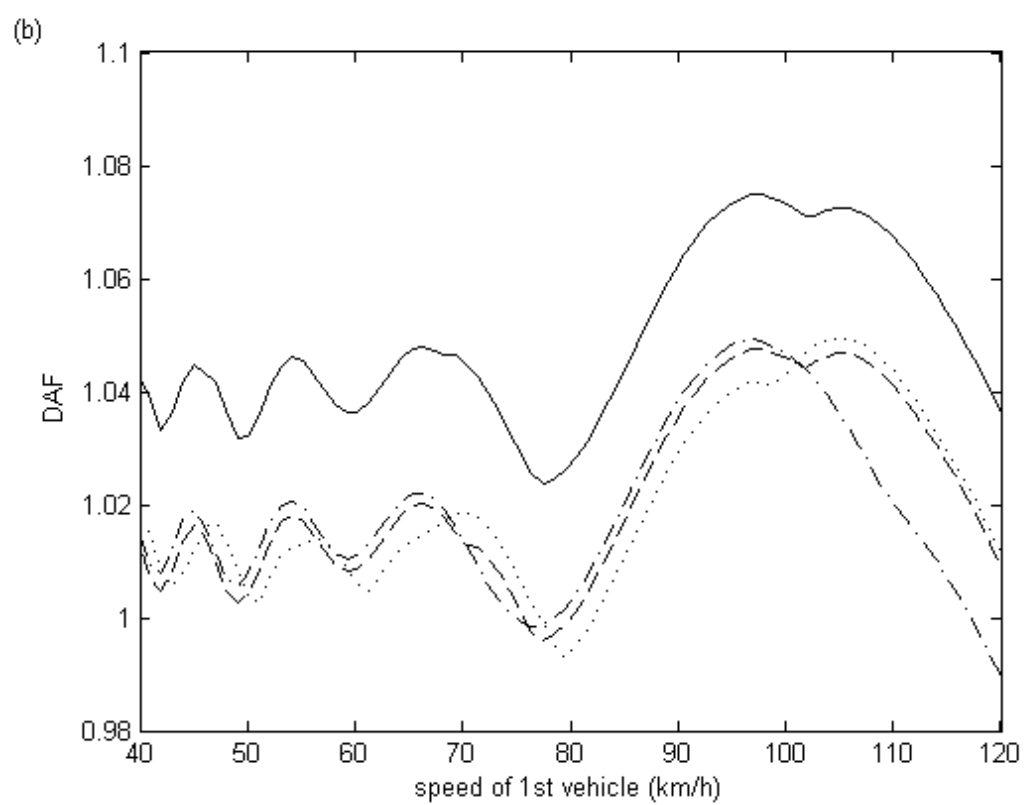
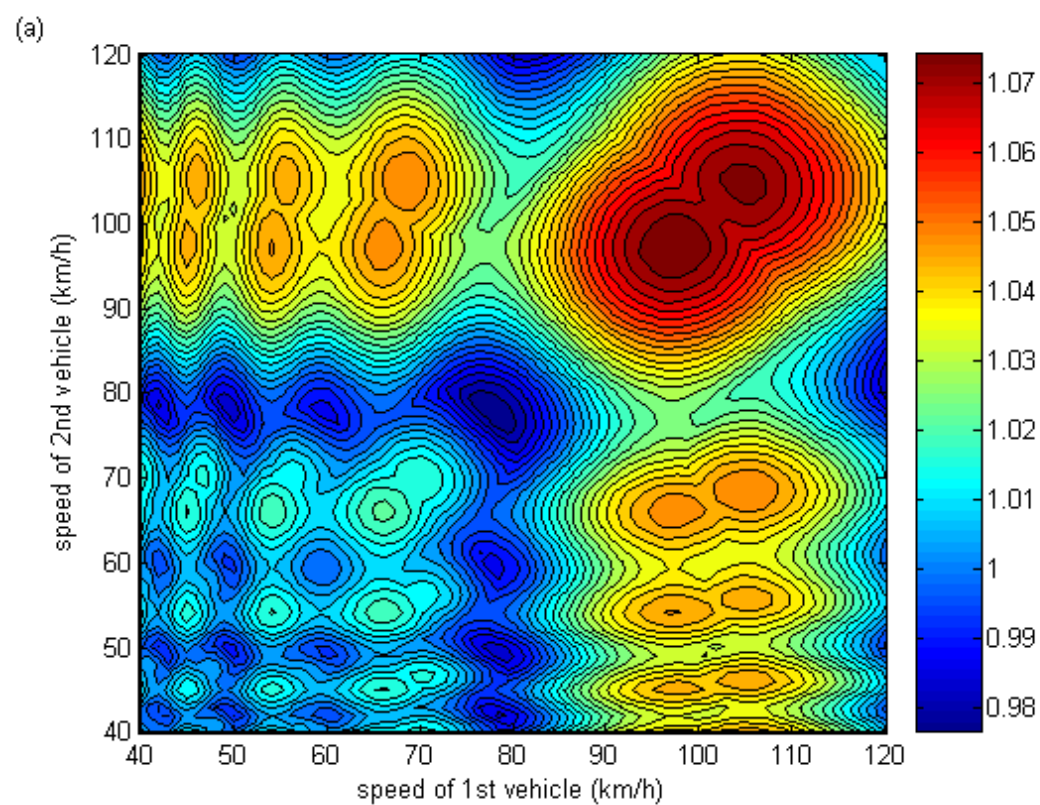


Figure 9

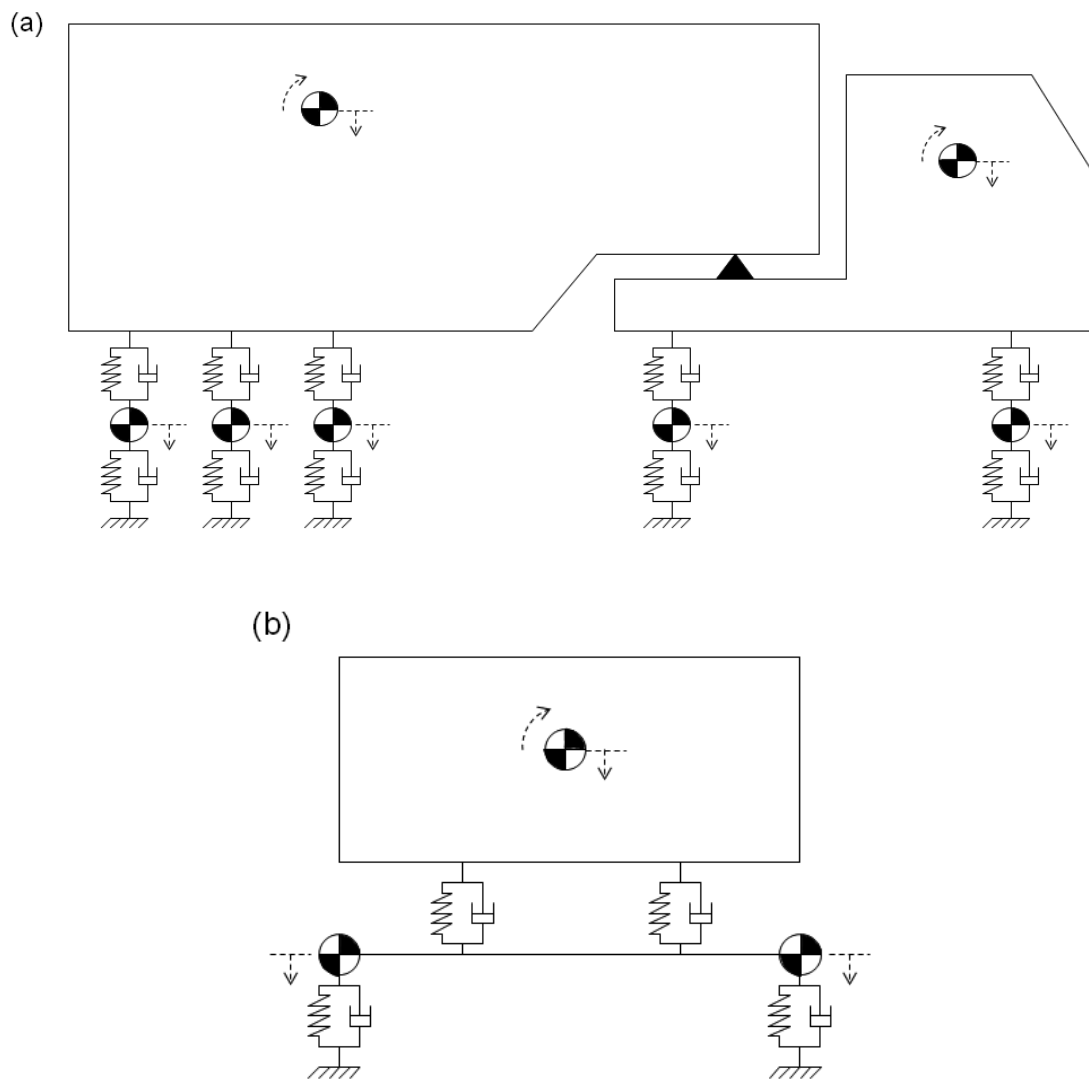


Figure 10

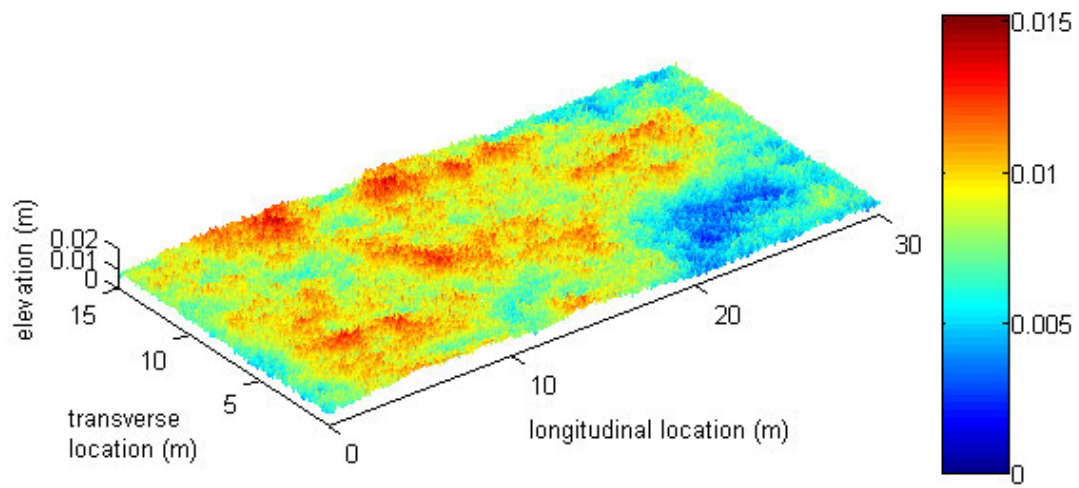


Figure 11

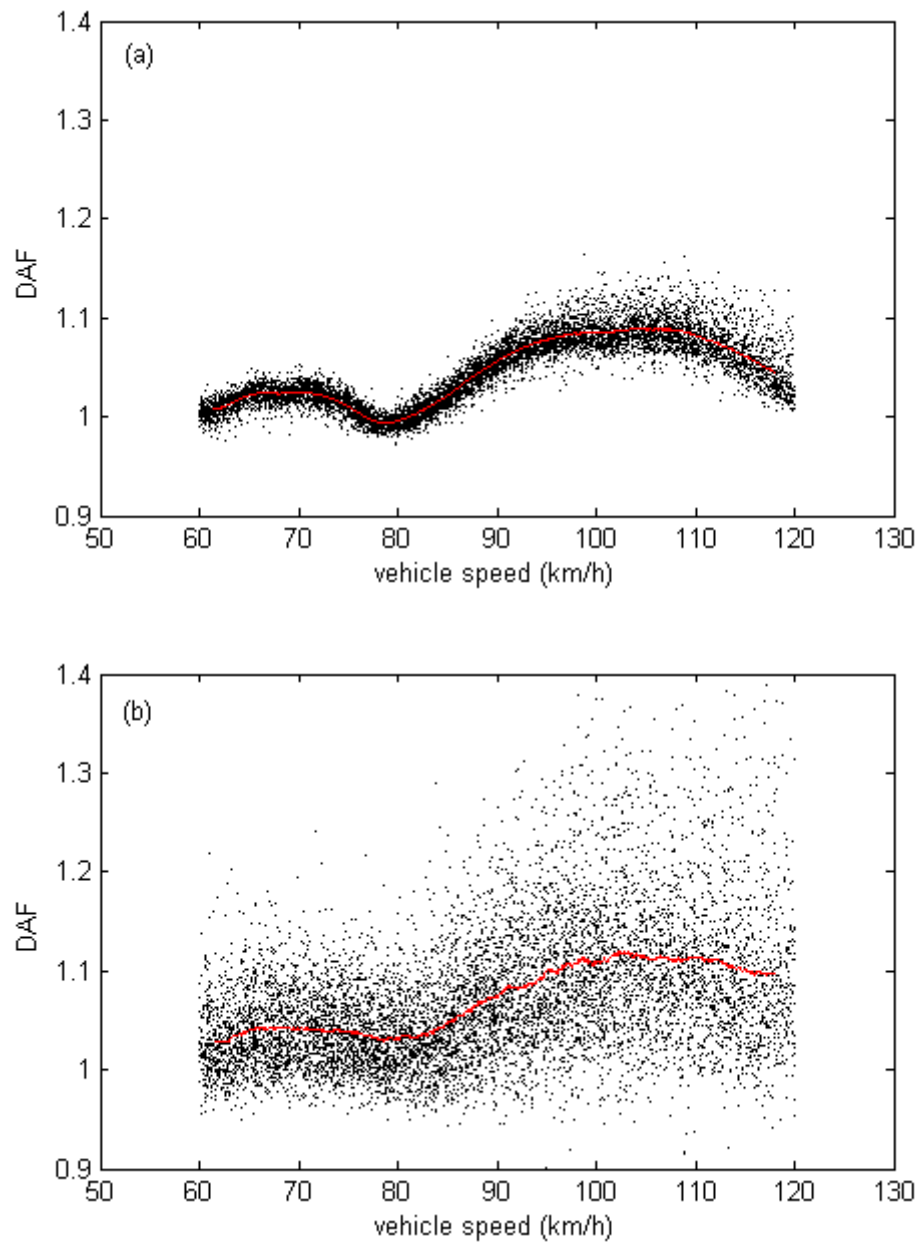


Figure 12

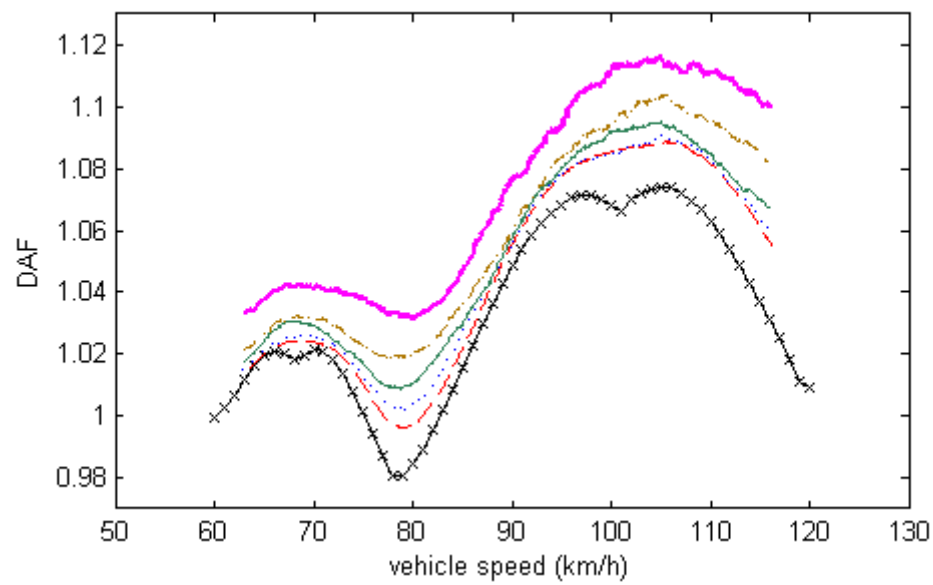


Figure 13

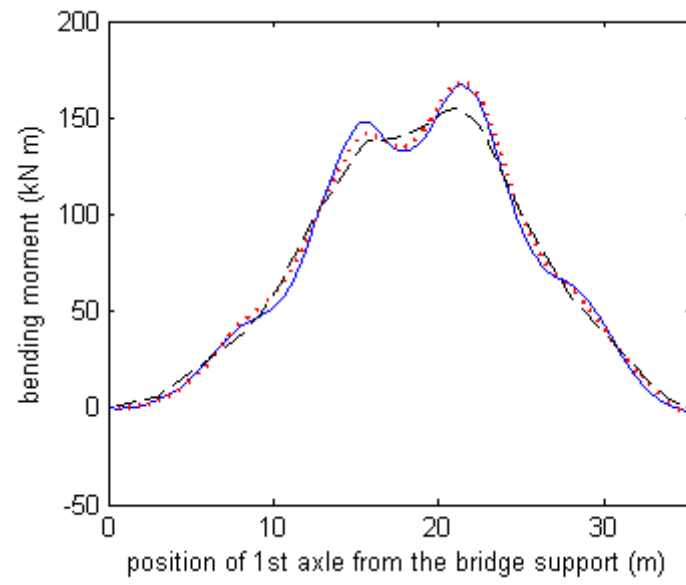


Figure 14

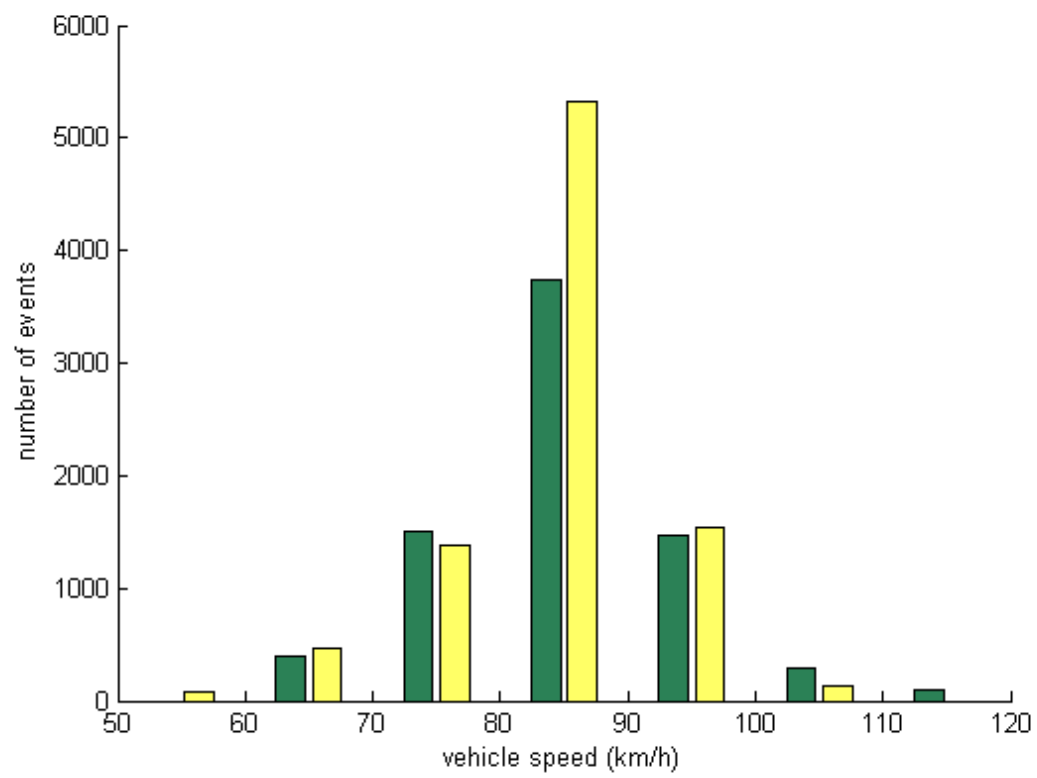


Figure 15

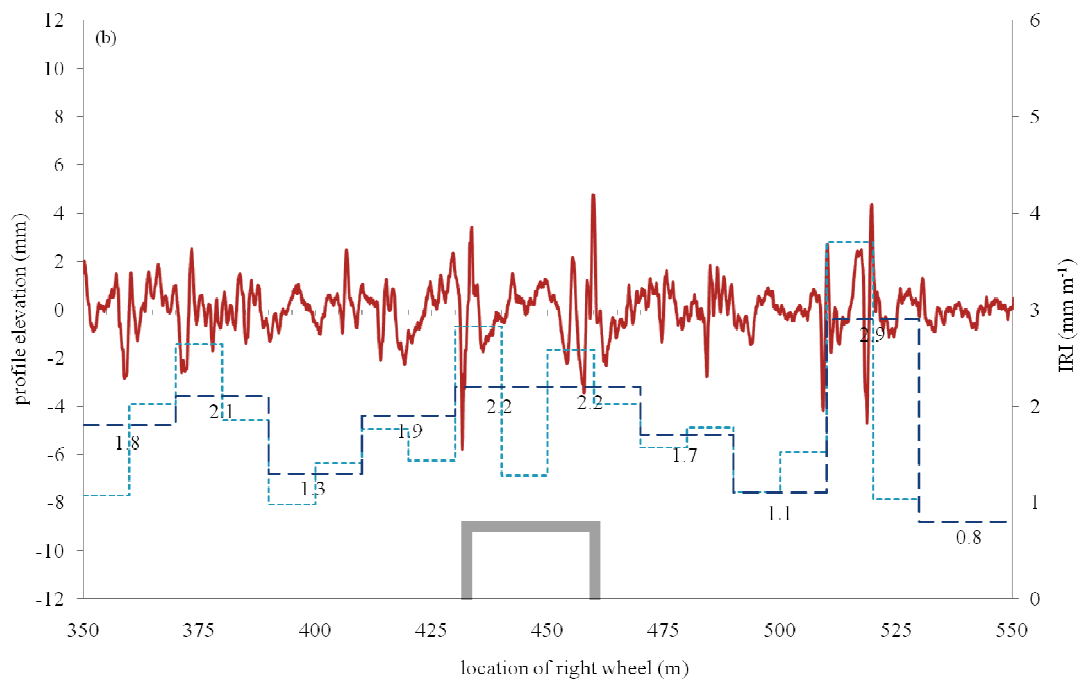
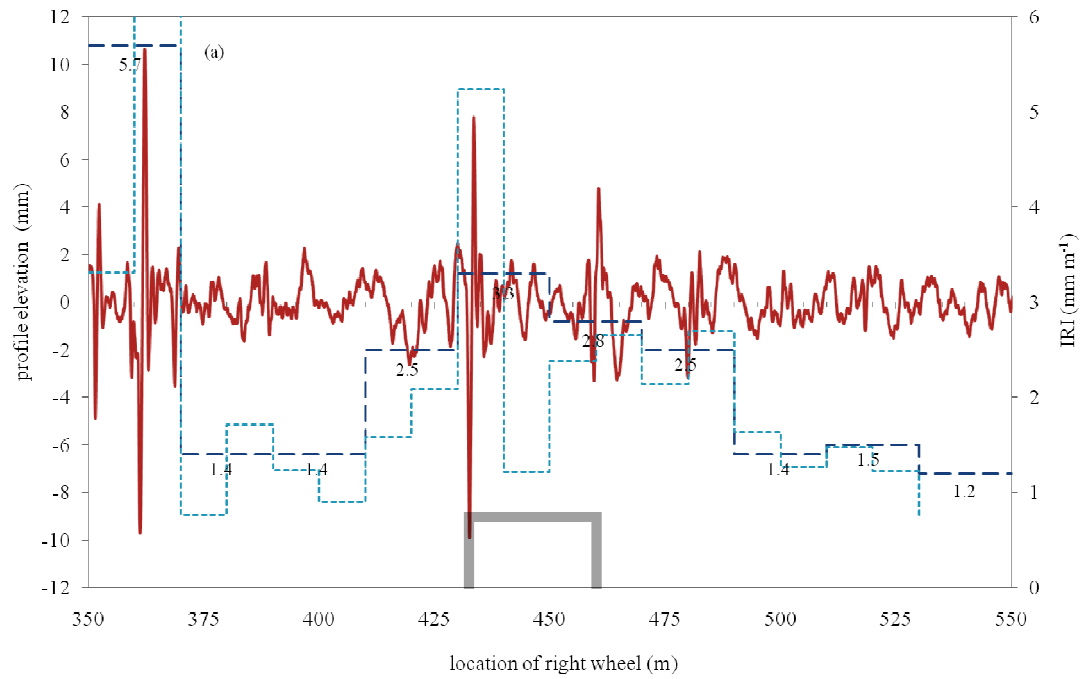


Figure 16



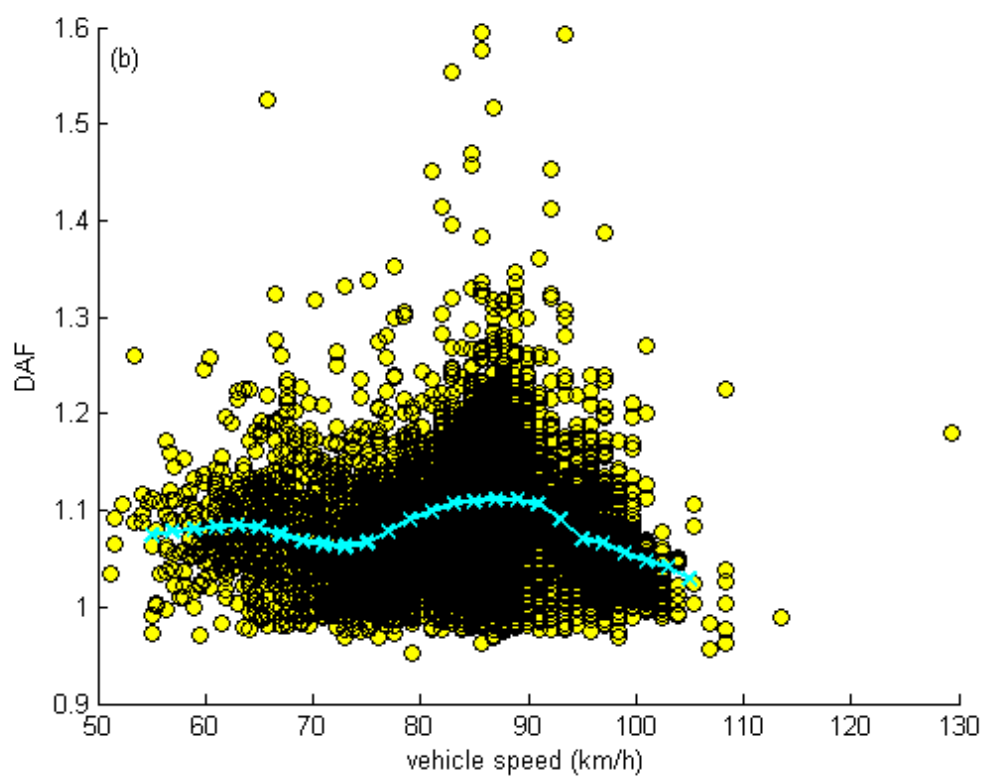
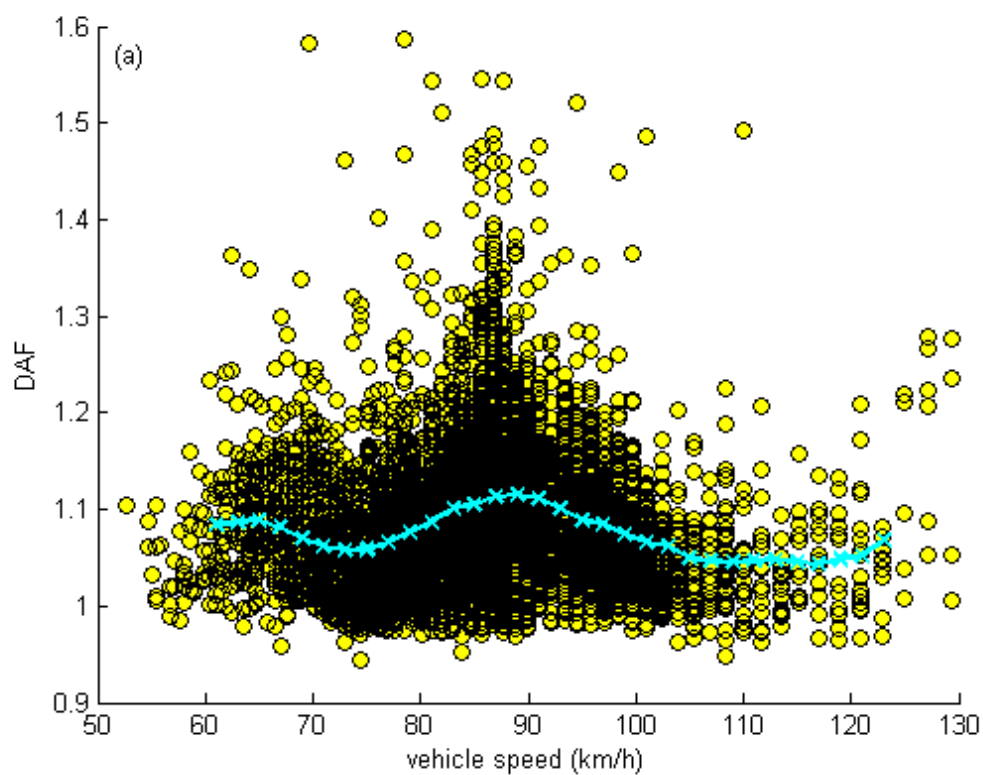


Figure 17

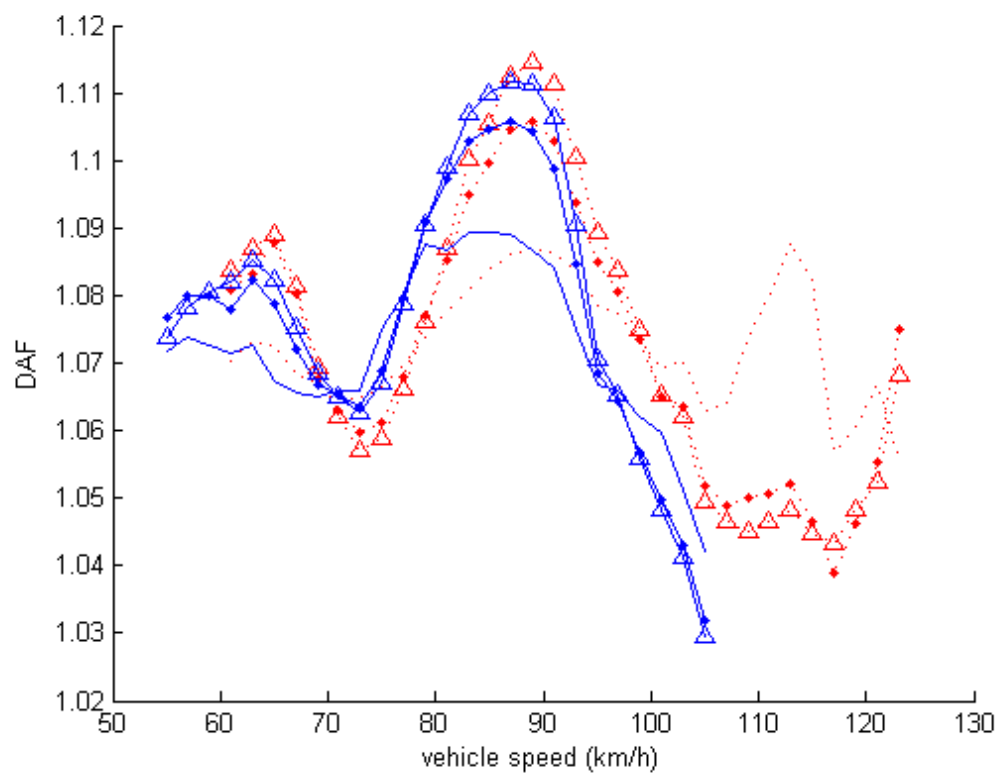


Figure 18

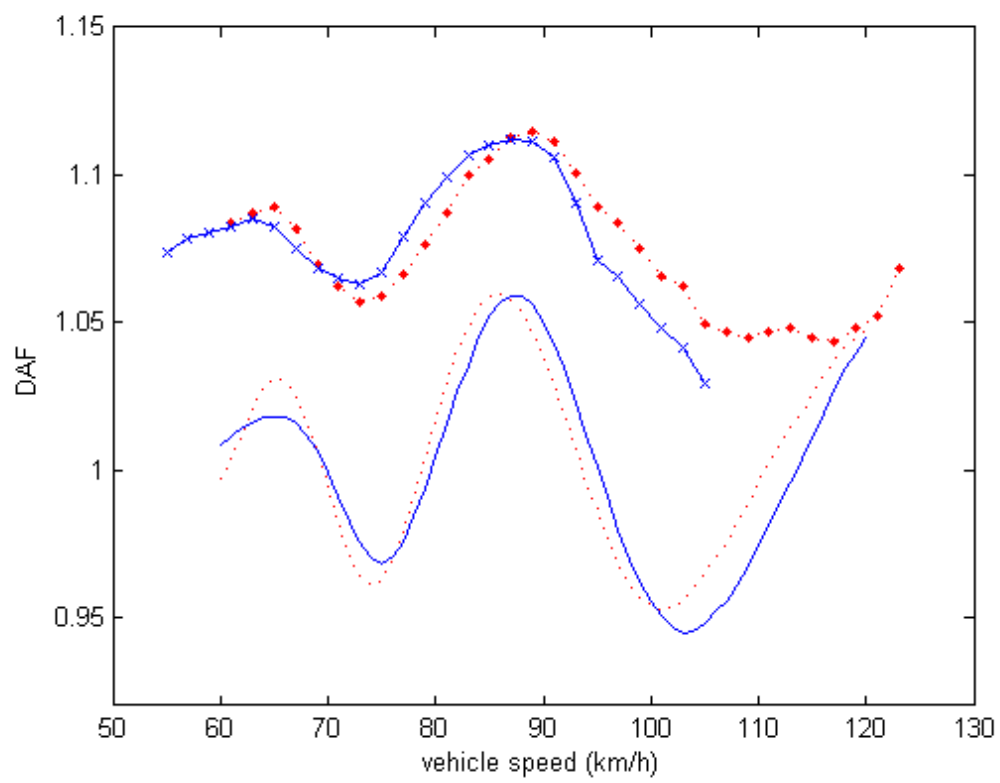


Figure 19